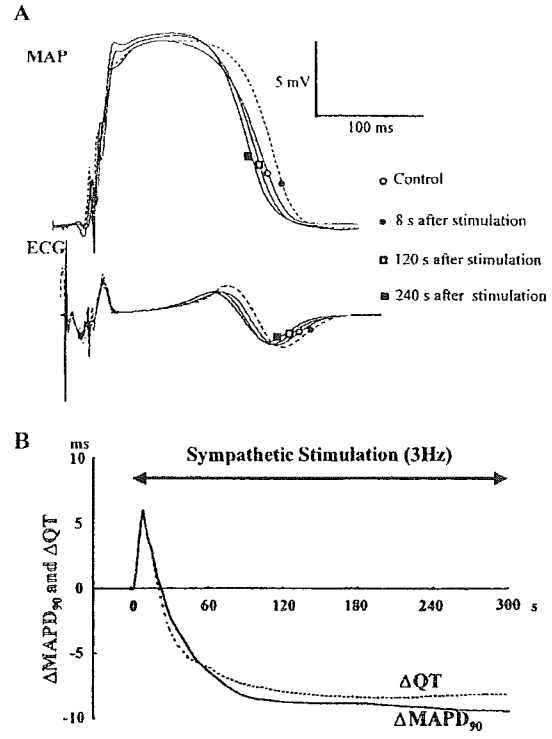

Fig 1. Dynamic response of the MAP and ECG to sudden sympathetic stimulation recorded from a representative case. (A) MAPs and ECGs recorded before (control) and 8 s, 120 s, and 240 s after stepwise sympathetic stimulation. Both the $MAPD_{90}$ and QT interval were transiently prolonged at 8 s after sympathetic stimulation, then gradually shortened (120 s and 240 s). (B) Transient response of $MAPD_{90}$ (solid line) and QT interval (broken line).

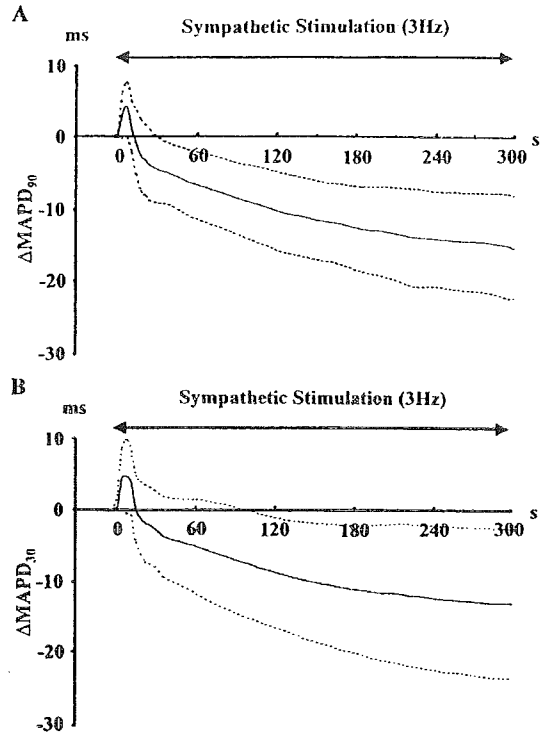

Fig 2. Dynamic changes in $MAPD_{90}$ ($\Delta MAPD_{90}$) (A) and $MAPD_{30}$ ($\Delta MAPD_{30}$) (B) in response to stepwise sympathetic stimulation (3 Hz). The solid line represents the mean and the broken lines represent ± SD.

to eliminate the effect of changing heart rate on APD. For recording of the MAP, a specially designed silver-silver chloride bipolar contact electrode catheter was inserted through the cervical vein and positioned with its tip electrode against the endocardium of the right ventricle![2]

Data Recording and MAP Analysis

The MAP, body surface electrocardiogram (ECG) and BP were continuously recorded during constant pacing at a cycle length of 350 ms. The MAP signals were amplified with a DC coupled differential amplifier (AB651J, Nihon Kohden, Tokyo, Japan) at a frequency range from 0.08 to 1,000 Hz. All data were digitized at 2,000 Hz with the aid of a 12-bit resolution analog-to-digital converter (AD12-16D (98)H, Contec, Osaka, Japan) hosted by a dedicated laboratory computer system (PC9801 FA, NEC, Tokyo, Japan). We measured MAP duration at 90% repolarization ($MAPD_{90}$) and at 30% repolarization ($MAPD_{30}$) in each beat using custom-made software. The error of measurement was ±0.5 ms.

Experiment Protocols

The dynamic changes of $MAPD_{90}$ in response to stepwise sympathetic stimulation were examined. After confirmation of stable MAP recording for 20 min, we stimulated both sympathetic nerves for 300 s. The standard deviation of $MAPD_{90}$ during the control recording (300 s) was 0.94 ms. Pulses used for the stimulation consisted of a square wave of 2 ms, 3 Hz, and 5 V. The sympathetic stimulation gradually increased the mean BP from 91.4±17.1 mmHg to 110.5±17.9 mmHg.

To clarify the contribution of the α- and β-adrenergic receptors to the transient and steady-state effects of sympathetic stimulation on $MAPD_{90}$, the responses of $MAPD_{90}$ to sympathetic stimulation were again determined after the administration of propranolol (0.5 mg/kg iv) (n=5) or phentolamine (1.0 mg/kg iv) (n=5).

Statistics

All data are expressed as mean±SD values. One-way repeated ANOVA was used to compare the response of $MAPD_{90}$ to sympathetic stimulation. The effects of phentolamine and propranolol on the $MAPD_{90}$ responses were examined by paired t test. The differences were considered significant at p-value <0.05.

Results

Dynamic Changes of $MAPD_{90}$ and QT Interval in Response to Sudden Stepwise Sympathetic Stimulation

Fig 1A shows representative tracings of the MAP and ECG in response to sympathetic stimulation. Compared with the control (pre-stimulation), both the $MAPD_{90}$ and QT interval were transiently prolonged after sympathetic stimulation (8 s after sympathetic stimulation), and then gradually shortened (120 s and 240 s after sympathetic stimulation). During sympathetic stimulation, neither early nor late afterdepolarization-like potentials were observed.

The dynamic changes in $MAPD_{90}$ ($\Delta MAPD_{90}$) in response to sympathetic stimulation are shown in Fig 1B. $MAPD_{90}$ was transiently prolonged by 5.7 ms at 8.0 s, and monotonically shortened toward a steady-state level (–9.3 ms). The QT interval was transiently prolonged by 5.9 ms at 8.0 s, and monotonically shortened toward a

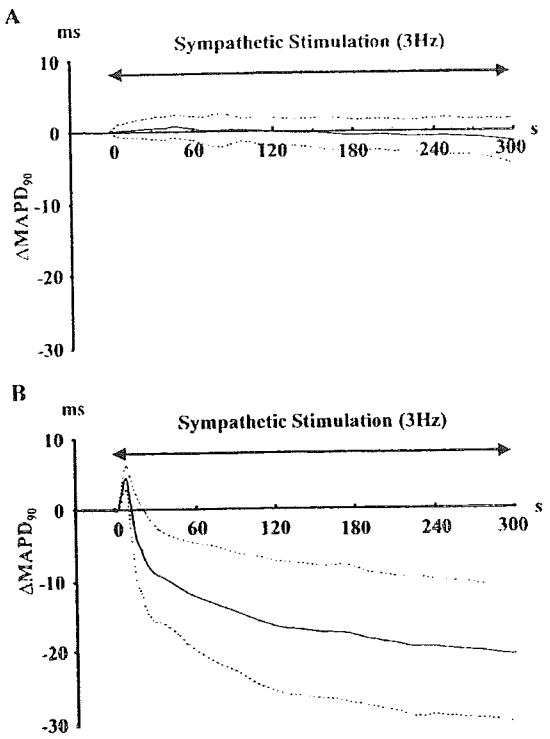

Fig 3. ΔMAPD90 in response to stepwise sympathetic stimulation (3 Hz) after the administration of autonomic nerve blockers. The solid line represents the mean and the broken lines represent ± SD. (A) After propranolol (0.5 mg/kg, iv), the changes in MAPD90 in response to sympathetic stimulation were not significant (n=5). (B) After phentolamine (1.0 mg/kg, iv), stepwise sympathetic stimulation transiently prolonged the MAPD90 and then shortened it toward a steady-state level in the same way as before phentolamine (n=5).

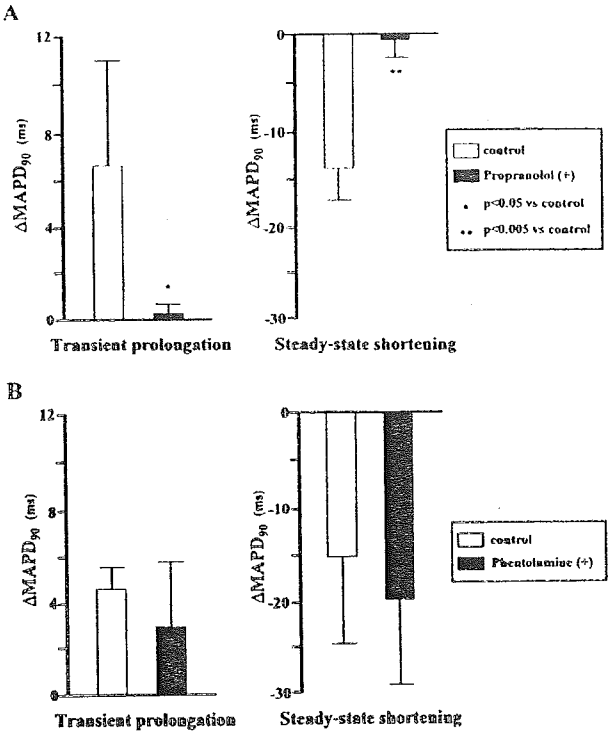

Fig 4. Effects of autonomic nerve blockade on the transient prolongation and steady-state shortening of MAPD90 after sympathetic stimulation. Values are mean ± SD. (A) Propranolol decreased both the transient prolongation (Left panel) and steady-state shortening (Right panel) (n=5). (B) Phentolamine did not attenuate either transient prolongation (Left panel) or steady-state shortening (Right panel) (n=5).

steady-state level (−7.8 ms). The transient response of the QT interval had a strong resemblance to that of the MAPD90 and this biphasic response of the MAPD90 and QT interval to stepwise sympathetic stimulation was consistently observed in all cats.

ΔMAPD90 and the dynamic changes in MAPD30 (ΔMAPD30) in response to sympathetic stimulation averaged over the 10 cats are shown in Fig 2. We quantified these changes by defining 'transient prolongation' as the maximal prolongation occurring within 15 s after sympathetic stimulation, and 'steady-state shortening' as the average response in the last 30 s of 300 s stimulation. In the pre-stimulation period, MAPD90 was 194.8±13.6 ms. MAPD90 was transiently prolonged by 5.5±3.2 ms (transient prolongation) ($p<0.01$ vs control) at 7.0±1.3 s, and monotonically shortened toward a steady-state level (steady-state shortening, −14.5±6.9 ms) ($p<0.0001$ vs control) (Fig 2A). MAPD30 was also prolonged by 4.8±5.2 ms (transient prolongation) ($p<0.01$ vs control) at 7.0±1.3 s, and monotonically shortened toward a steady-state level (steady-state shortening, −12.6±10.3 ms) ($p<0.0001$ vs control) (Fig 2B).

Contribution of α- and β-Adrenergic Receptor to the Transient and Steady-State Effects of Sympathetic Stimulation on MAPD90

The dynamic changes in MAPD90 in response to stepwise sympathetic stimulation after the administration of α- (phentolamine, 1.0 mg/kg iv) and β-blockade (propranolol, 0.5 mg/kg iv) are shown in Fig 3. Propranolol abolished both the transient prolongation and steady-state shortening (Fig 3A), but phentolamine did not affect either of these parameters (Fig 3B).

Propranolol markedly attenuated the transient prolongation (6.6±4.5 to 0.2±0.4 ms, $p<0.05$) and steady-state shortening (−13.7±3.6 to −1.1±2.4 ms, $p<0.005$) (Fig 4A). Phentolamine altered neither (4.5±0.9 to 2.9±3.1 ms, NS and −15.3±9.6 to −20.2±9.4 ms, NS, respectively) (Fig 4B).

Discussion

We demonstrated a biphasic response of the APD to stepwise sympathetic stimulation; that is, the APD was transiently prolonged for approximately 15 s and then gradually shortened toward a steady-state level. Beta-adrenergic blockade totally abolished both the transient prolongation and the steady-state shortening of APD.

Transient Prolongation of APD in Response to Stepwise Sympathetic Stimulation

Although previous studies have reported steady-state shortening of the APD in response to sympathetic stimulation[7,13] the dynamic response of the APD to sympathetic stimulation has not been fully defined. Some experimental and clinical studies reported a transient response of repolarization to sympathetic stimulation, but they used a brief sympathetic nerve stimulation or rapid catecholamine injection as the input stimulation, which makes it difficult to quantitatively characterize the dynamic response of APD. In the present study, we quantitatively characterized the dynamic response of the APD to sympathetic stimula-

tion by using a stepwise stimulation method.

Experimental and clinical studies have shown transient prolongation of the QT interval in response to adrenergic stimulation[14–16] Abildskov showed in dogs that either rapid injection of catecholamine or brief (2–3 s) sympathetic stimulation was followed by transient prolongation of the QT interval, whereas slow injection of catecholamine or long (1–5 min) sympathetic stimulation was followed by a shortening of the QT interval[14] Coghlan et al reported the existence of a paradoxical early lengthening and subsequent shortening of the QT interval in response to exercise in patients with pacemaker implantation[15] As a mechanism of the transient QT interval prolongation caused by adrenergic stimulation, it has been postulated that rapid injection of catecholanime or brief sympathetic stimulation are likely to shorten the APD at localized sites and prolong the QT interval by exposing the ECG effects of other sites that have been cancelled[14,16] On the other hand, Murayama et al showed that brief (3 s) satellate stimulation prolonged the APD in dogs[17] and the results of the present study indicate that stepwise sympathetic stimulation substantially prolongs the APD. We propose that transient QT prolongation after adrenergic stimulation is caused by both substantial APD prolongation and the unmasking of the repolarization force, which previously cancelled each other.

Our findings were basically in accordance with the observations made by Abildskov[14] and Coghlan et al[15] The precise response of the APD to sympathetic stimulation, however, was slightly different from that of the QT interval. Brief sympathetic stimulation or rapid injection of catecholamine prolonged the QT interval by 10–30 ms in the study of Abildskov[14] but the transient prolongation of the APD after sympathetic stimulation was 5.5±3.2 ms in the present study. The QT interval was prolonged at the first minute of exercise in the study of Coghlan et al[15] but the shortening of the APD occurred within the first minute of our study. Such differences may be related to the different ways of inducing sympathetic activation and quantifying repolarization.

Mechanism of the Transient Prolongation of the APD

We considered that the hemodynamic effect was not a major factor in the APD prolongation because its onset preceded the increase in BP following sympathetic stimulation.

Beta-blockade abolished both the transient prolongation and steady-state shortening of the APD after sympathetic stimulation. Alpha-blockade, however, had no significant effects on either, which indicates that the transient and steady-state response of APD to stepwise sympathetic stimulation are mediated through the β-adrenergic receptor, with minimal contribution of the α-adrenergic receptor.

Although α-adrenergic stimulation has the potential to prolong repolarization by decreasing the transient outward current (I_{to}) and the delayed rectifier current (I_K)[18,19] our findings suggest that β-adrenergic stimulation transiently prolonged APD. The effects of β-adrenergic stimulation are mainly mediated by the activation of the adenylate cyclase-cAMP second messenger system via the GTP-binding protein (G protein)[19–22] The activation of this system markedly affects the major ionic currents, such as the inward Ca^{2+} currents (I_{Ca}), I_{Ks} and I_{Kr}, and I_{to}[19,20,23] The net effect of these ionic currents determines the effect of β-adrenergic stimulation on repolarization and it is generally recognized that the net effect of β-stimulation is to accelerate repolarization;[19,20] however, the dynamic response of repolarization to β-stimulation has not been completely defined. In the present study, sympathetic stimulation transiently prolonged the $MAPD_{30}$ to the same extent as the $MAPD_{90}$, which suggests that ionic currents activated during the plateau phase play an important role in the prolongation of the APD. The time constant of I_{Ca} modulation by the adenylate cyclase-cAMP second messenger system might be shorter than that of I_{Ks}. Furthermore, it has been reported that a G protein stimulates I_{Ca} by both a membrane-delimited pathway (direct pathway) and an adenylate cyclase-cAMP second messenger pathway (indirect pathway)[24–26] The time constant of ionic current modulation by a direct pathway is shorter than that by an indirect pathway[25]

We conjecture that the difference in the time courses of the various ionic current changes induced by β-adrenergic stimulation produces the biphasic response of the APD to sympathetic stimulation. Further studies are needed to clarify the mechanisms involved in the transient prolongation of the APD by sympathetic stimulation.

Clinical Implications

Although activation of the sympathetic nervous system has been suggested as an important factor in the genesis of life-threatening arrhythmias and sudden death[3,6,27] the precise mechanisms remain unclear. Our findings provide a clue to the mechanisms involved in life-threatening arrhythmias that develop immediately after sudden sympathetic activation.

Harris et al found that in dogs the arrhythmias following stimulation of the ansa subclavia, in the presence of coronary occlusion, usually had their onset approximately 10 s after stimulation[28] Wellens et al[10] and Wilde et al[11] reported that patients with congenital long QT syndrome suffered from torsade de pointes at 6–10 s after the sound of an alarm clock. Such timing is in good agreement with the phase of transient prolongation in the present study, suggesting a relationship between the period of APD prolongation and arrhythmias. The transient prolongation of APD would favor the onset of arrhythmias through various mechanisms. In the inhomogeneously denervated ventricle, such as after myocardial infarction[29] the transient prolongation of the APD by sudden sympathetic activation would be spatially heterogeneous and that heterogeneous prolongation of the APD would increase the spatial dispersion of the refractory period and provide a substrate for reentry[30] Moreover, the transient prolongation of the APD would increase the instability of ventricular repolarization and facilitate triggered activity. On the other hand, the homogeneous prolongation of the APD may act as an antiarrhythmic factor; however, clinical studies report that prolongation of repolarization is associated with an adverse prognosis in patients with organic heart disease[31,32]

Ample clinical evidence supports the usefulness of β-blockade in preventing sudden cardiac death[33–35] and we conjecture that the attenuation of both the transient prolongation and the steady-state shortening of the APD partially explains the effect of β-blockade.

Study Limitations

First, we used MAP for quantifying repolarization, but the MAP, which is a multicellular recording, reflects electrical activity integrated over a substantial area. Thus, the transient prolongation of the MAPD may be caused by the unmasking of repolarization forces that previously cancelled each other, in the same way as the paradoxical QT

prolongation in the body surface ECG. Experimental studies, however, have shown that the MAP does reflect electrical activity from a very small area, not more than 5 mm in diameter, and reproduces the time course of the repolarization of transmembrane action potentials with high fidelity under various conditions![12,36] Therefore, we believe there is little possibility that local shortening of the APD causes the prolongation of MAPD. Second, the stepwise sympathetic stimulation used in this study may be 'unphysiological' and studies of the dynamic APD changes after physiological stress may be necessary. Third, although we demonstrated transient prolongation of the APD after sympathetic stimulation, we have not determined whether these changes in the APD actually render the heart vulnerable. In particular, because the transient prolongation is less than the steady-state shortening, the clinical importance of the transient prolongation should be investigated. Fourth, this study was performed under anesthetized and decentralized conditions. In the physiological condition, concomitant parasympathetic nervous activity may alter the effects of sudden sympathetic activation on the APD.

Conclusion

This study demonstrated that sudden sympathetic stimulation transiently prolonged and then gradually shortened the APD. The transient prolongation of the APD after sudden sympathetic activation might play a role in the genesis of life-threatening arrhythmias by favoring reentry and triggered activity. Beta-blockade diminished both the transient prolongation and steady-state shortening of the APD.

Acknowledgments

This study was supported by the Program for Promotion of Fundamental Studies in Health Science of the Organization for Pharmaceutical Safety and Research of Japan, the Development for Applying Advanced Computational Science and Technology, Japan Science and Technology Corporation, Nakatani Electronic Measuring Technology Association of Japan and the Fukuda Foundation for Medical Technology

References

1. Huikuri HV, Castellanous A, Myerbrg RJ. Sudden death due to cardiac arrhythmias. *N Engl J Med* 2001; **345:** 1473–1482.
2. Zheng ZJ, Croft JB, Giles WH, Mensah GA. Sudden cardiac death in the United States, 1989–1998. *Circulation* 2001; **104:** 2158–2163.
3. Coumel P, Leenhardt A. Mental activity, adrenergic modulation, and cardiac arrhythmias in patients with heart disease. *Circulation* 1991; **83**(Suppl II): 58–70.
4. Han J, Jalon PG, Moe GK. Adrenergic effects on ventricular vulnerability. *Circ Res* 1964; **14:** 516–524.
5. Lown B. Sudden cardiac death: Biobehavioral perspective. *Circulation* 1987; **76**(Suppl I): 186–196.
6. Podrid PJ, Fuchs T, Candinas R. Role of the sympathetic nervous system in the genesis of ventricular arrhythmia. *Circulation* 1990; **82**(Suppl I): 103–113.
7. Matoba T, Toshima H, Nagae K, Yamazaki S. Changes of ventricular monophasic action potential duration by stellate ganglion stimulation in dogs. *Jpn Heart J* 1979; **20:** 477–484.
8. Garcia-Calvo R, Chorro FJ, Sendra M, Alberola A, Sanchis J, Navarro J, et al. The effects of selective stellate ganglion manipulation on ventricular refractoriness and excitability. *Pacing Clin Electrophysiol* 1992; **15:** 1492–1503.
9. Martins JB, Zipes DP. Effects of sympathetic and vagal nerves on recovery properties of the endocardium and epicardium of the canine left ventricle. *Circ Res* 1980; **46:** 100–110.
10. Wellens HJ, Vermeulen A, Durrer D. Ventricular fibrillation occurring on arousal from sleep by auditory stimuli. *Circulation* 1972; **46:** 661–665.
11. Wilde AA, Jongbloed RJ, Doevendans PA, Duren DR, Hauer RN, van Langen IM, et al. Auditory stimuli as a trigger for arrhythmic events differentiate HERG-related (LQTS2) patients from KVLQT1-related patients (LQTS1). *J Am Coll Cardiol* 1999; **33:** 327–332.
12. Franz MR. Current status of monophasic action potential recording: Theories, measurements and interpretations. *Cardiovasc Res* 1999; **41:** 25–40.
13. Priori SG, Mantica M, Schwartz PJ. Delayed afterdepolarizations elicited in vivo by left stellate ganglion stimulation. *Circulation* 1988; **78:** 178–185.
14. Abildskov JA. Adrenergic effects of the QT interval of the electrocardiogram. *Am Heart J* 1976; **92:** 210–216.
15. Coghlan JG, Madden B, Norell MN, Ilsley CD, Mitchell AG. Paradoxical early lengthening and subsequent linear shortening of the QT interval in response to exercise. *Eur Heart J* 1992; **13:** 1325–1328.
16. Yanowitz F, Preston JB, Abildskov JA. Functional distribution of right and left stellate innervation to the ventricles: Production of neurogenic electrocardiographic changes by unilateral alteration of sympathetic tone. *Circ Res* 1966; **18:** 416–428.
17. Murayama M, Harumi K, Mashima S, Shimomura K, Murao S. Prolongation of ventricular action potential due to sympathetic stimulation. *Jpn Heart J* 1977; **18:** 259–265.
18. Apkon M, Nerbonne JM. α1-adrenergic agonists selectively suppress voltage dependent K^+ currents in rat ventricular myocytes. *Proc Natl Acad Sci USA* 1988; **85:** 8756–8760.
19. Rosen MR, Jeck CD. Autonomic modulation of cellular repolarization and of the electrocardiographic QT interval. *J Cardiovasc Electrophysiol* 1992; **3:** 487–499.
20. Lindemann JP, Watanabe AM. Sympathetic control of cardiac electrical activity. *In*: Zipes DP, Jalife J, editors. Cardiac electrophysiology from cell to bedside. Philadelphia: Saunders; 1990: 277–283.
21. Steinberg SF. The molecular basis for distinct β-adrenergic receptor subtype actions in cardiomyocytes. *Circ Res* 1999; **85:** 1101–1011.
22. Wickman K, Clapham DE. Ion channel regulation by G proteins. *Physiol Rev* 1995; **75:** 865–885.
23. Christoph AK, Edgar Z, Wei Z, Sven K, Wolfgang S, Johann K. Rapid component I_{Kr} of the guinea-pig cardiac delayed rectifer K^+ current is inhibitted by beta 1 adrenoreceptor activation, via cAMP/protein kinase A-dependent pathway. *Cardiovasc Res* 2002; **53:** 355–362.
24. Shuba YM, Hesslinger B, Trautwein W, McDonald TF, Pelzer D. Whole-cell calcium current in guinea-pig ventricular myocytes dialysed with guanine nucleotides. *J Physiol (Lond)* 1990; **424:** 205–228.
25. Yatani A, Brown AM. Rapid β-adrenergic modulation of cardiac calcium channel currents by a fast G protein pathway. *Science* 1989; **245:** 71–74.
26. Yatani A, Tajima Y, Green SA. Coupling of β-adrenergic receptors to cardiac L-type Ca^{2+} channels: Preferential coupling of the β_1 versus β_2 receptor subtype and evidence for PKA-independent activation of the channel. *Cell Signal* 1999; **11:** 337–342.
27. Kinugawa T, Ogino K, Osaki S, Kato M, Igawa O, Hisatome I, et al. Prognostic significance of exercise plasma noradrenaline levels for cardiac death in patients with mild heart failure. *Circ J* 2002; **66:** 261–266.
28. Harris AS, Otero H, Bocage AJ. The induction of arrhythmias by sympathetic activity before and after occlusion of a coronary artery in the canine heart. *J Electrocardiol* 1971; **4:** 34–43.
29. Ando M, Yamabe H, Sakurai K, Kawai H, Yokoyama M. Relationship between cardiac sympathetic function and baroreceptor sensitivity after acute myocardial infarction. *Circ J* 2002; **66:** 247–252.
30. Nanke T, Nakazawa K, Arai M, Ryuu S, Osada K, Sakurai T, et al. Clinical significance of the dispersion of the activation-recovery interval and recovery time as markers for ventricular fibrillation susceptibility in patients with Brugada syndrome. *Circ J* 2002; **66:** 549–552.
31. Davey P. QT interval and mortality from coronary artery disease. *Prog Cardiovasc Dis* 2000; **42:** 359–384.
32. Padmanabhan S, Silvet H, Amin J, Pai RG. Prognostic value of QT interval and QT dispersion in patients with left ventricular systolic dysfunction: Results from a cohort of 2265 patients with an ejection fraction of ≤40%. *Am Heart J* 2003; **145:** 132–138.
33. Hjalmarson A. Effects of beta blockade on sudden cardiac death during acute myocardial infarction and the postinfarction period. *Am J Cardiol* 1997; **80:** 35J–39J.
34. Congestive heart failure. *Am J Cardiol* 1999; **84:** 94R–102R.
35. Yusuf S, Peto R, Lewis J, Collins R, Sleight P. Beta blockade during and after myocardial infarction: An overview of the randomized trials. *Prog Cardiovasc Dis* 1985; **27:** 335–371.
36. Ino T, Karagueuzian HS, Hong K, Meesmann M, Mandel WJ, Peter T. Relation of monophasic action potential recorded with contact electrode to underlying transmembrane action potential properties in isolated cardiac tissues: A systematic microelectrode validation study. *Cardiovasc Res* 1988; **22:** 255–264.

Japanese Journal of Physiology, 53, 461–466, 2003

Carotid-Sinus Baroreflex Modulation of Core and Skin Temperatures in Rats: An Open-Loop Approach

Dongmei ZHANG, Motonori ANDO, Fumiyasu YAMASAKI*, and Takayuki SATO

Department of Cardiovascular Control, and * Department of Clinical Laboratory, Kochi Medical School, Nankoku, 783–8505 Japan

Abstract: The neural mechanisms of the thermoregulatory control of core and skin temperatures in response to heat and cold stresses have been well clarified. However, it has been unclear whether baroreceptor reflexes are involved in the control of core and skin temperatures. To investigate how the arterial baroreceptor reflex modulates the body temperatures, we examined the effect of pressure changes of carotid sinus baroreceptors on core and skin temperatures in halothane-anesthetized rats. To open the baroreflex loop and control arterial baroreceptor pressure (BRP), we cut vagal and aortic depressor nerves and isolated carotid sinuses. We sequentially altered BRP in 20-mmHg increments from 60 to 180 mmHg and then in 20-mmHg decrements from 180 to 60 mmHg while measuring systemic arterial pressure (SAP), heart rate (HR), and core blood temperature (T_{core}) at the aortic arch and skin temperature (T_{skin}) at the tail. In response to the incremental change in BRP by 120 mmHg, SAP, HR, and T_{core} fell by 90.3±5.1 mmHg, 60.3±10.5 beats min^{-1}, and 0.18±0.01°C, respectively. T_{skin} rose by 0.84±0.10°C. The maximum rate of change per unit BRP change was −2.1±0.2 for SAP, −1.5±0.4 beats min^{-1} $mmHg^{-1}$ for HR, −0.003±0.001°C $mmHg^{-1}$ for T_{core}, and 0.011±0.002°C $mmHg^{-1}$ for T_{skin}. After the administration of hexamethonium or bretylium, these baroreflexogenic responses were completely abolished. We concluded that T_{core} and T_{skin} are modulated by the arterial baroreceptor reflex. [The Japanese Journal of Physiology 53: 461–466, 2003]

Key words: baroreflex, open loop, temperature.

The sympathetic nervous system plays an important role in a short-term control of body temperature. The rate of heat transfer from the body interior to the surface is regulated by the sympathetic manipulation of the skin blood flow. The neural mechanisms of thermoregulatory control of skin temperature in response to heat and cold stresses have been clarified [1–3]. However, it has been unclear whether baroreceptor reflexes are involved in the control of skin temperature.

The neurophysiological studies indicated that electrical stimulation of the carotid sinus nerve [4] and the pharmacological modulation of arterial pressure [5] failed to change the skin sympathetic nerve activity. It is also indicated that carotid baroreceptor unloading had no effect on skin blood flow in humans [6]. On the other hand, there is literature demonstrating that hemorrhaging is clearly associated with cutaneous vasoconstriction through sympathetic activation in mice [7], rats [8–11], rabbits [12, 13], and dogs [14]. However, its mechanism for hemorrhage-induced skin vasoconstriction still remains controversial.

Earlier human studies showed that nonhypotensive lower body negative pressure increased the skin vascular resistance, suggesting the importance of the cardiopulmonary, and not arterial, baroreceptor reflex in the regulation of cutaneous vasomotor tone [15–17]. However, Ryan *et al.* [13] indicated that ear vascular resistance during caval occlusion-induced hypotension decreased in intact rabbits but not in sinoaortic-denervated rabbits, suggesting the crucial role of the arterial baroreceptor reflex in the regulation of ear blood flow and heat transfer to the ear.

The controversies on the role of the baroreceptor reflex in skin circulation and on the interaction between

Received on October 17, 2003; accepted on November 26, 2003
Correspondence should be addressed to: Takayuki Sato, Department of Cardiovascular Control, Kochi Medical School, Nankoku, 783–8505 Japan. Tel: +81–88–880–2309, Fax: +81–88–880–2310, E-mail: tacsato-kochimed@umin.ac.jp

the baroreceptor and thermoregulatory reflexes would result from differences in experimental preparations. Although the effect of the cardiopulmonary baroreceptor reflex on thermoregulation was examined by the use of lower body negative pressure for unloading the cardiopulmonary baroreceptor, such a manipulation would inevitably produce changes in cardiac output according to the Frank-Starling law of the heart. Therefore it would be difficult to directly link the baroreceptor unloading to the resultant decrease in skin blood flow and temperature, because the decrease in cardiac output itself can directly modulate skin circulation. It is also difficult to evaluate the role of the arterial baroreceptor reflex in thermoregulation from the responses of core and skin temperatures to pharmacological changes in arterial pressure [18–20] because the systemic administration of vasoactive agents itself could affect the distribution of cardiac output to various organs, including the skin.

Along with thermoregulation, the baroreflex control of arterial pressure is a physiological feedback system. It is therefore complicated to clarify the effect of one regulatory system on another under experimental conditions in which the feedback loops of both systems are closed. In terms of systems physiology, an open-loop approach seems suitable for the elucidation of the effect of the baroreflex on thermoregulation. Our previous studies [21–24] developed experimental procedures for the isolation of arterial baroreceptor regions and equipment for the precise control of baroreceptor pressure in rats. In the present study, we characterized how the arterial baroreceptor reflex modulated core and skin temperatures under the open-loop conditions of the arterial baroreflex. We measured the central blood temperature at the ascending aorta as core temperature and monitored the skin temperature at the tail of the rat.

METHODS

Animals and surgical procedures. All experiments were performed in strict accordance with the Guiding Principles for the Care and Use of Animals in the Field of Physiological Science by the Physiological Society of Japan. Male Wistar rats (SLC, Hamamatsu, Japan) weighing 280–350 g were used. The temperature and humidity in an experimental room were continuously maintained in the ranges of 26–27°C and 40–45%. After an induction of anesthesia, an endotracheal tube was introduced orally, and the rat was ventilated artificially via a volume-controlled rodent respirator (model 693; Harvard Apparatus, South Natick, MA, USA). In accordance with Ono *et al.* [25], the rat was anesthetized with inspiration of 1.2% halothane during surgical procedures and 0.6% halothane during data recording. For the measurement of systemic artery pressure (SAP), a polyethylene tubing (PE-50; Becton Dickinson, Parsippany, NJ, USA) was inserted into the right femoral artery. For the prevention of dehydration during experiments [26] and the elimination of spontaneous muscle activity, physiologic saline ($5\,ml\,kg^{-1}\,h^{-1}$) and pancuronium bromide ($0.8\,mg\,kg^{-1}\,h^{-1}$) was continuously administered into the left femoral vein with a syringe pump (CFV-3200; Nihon Kohden, Tokyo, Japan). The temperature of the infusate was kept at 37°C with an in-line heating system (SF-28; Warner Instruments, Hamden, CT, USA).

As described previously [23], we isolated bilateral carotid sinus baroreceptor regions. After the vagi and the aortic depressor nerves were cut, the external carotid arteries were briefly ligated at the root of the bifurcation of the common carotid arteries, and the internal carotid and pterygopalatine arteries were then embolized with two ball bearings of 0.8 mm diameter. Two short polyethylene tubes (PE-50) were placed into both carotid sinuses and connected to a fluid-filled transducer (DX-200; Viggo-Spectramed, Singapore) and to a custom-made servocontrolled pump system based on an electromagnetic shaker and power amplifier (ARB-126; AR Brown, Osaka, Japan). We used the servopump to impose any desired pressure on carotid sinus baroreceptors.

To measure the core temperature (T_{core}), i.e., the central blood temperature, we placed a catheter-tip thermocouple (PTI-200; Unique Medical, Tokyo, Japan) in the ascending aorta via the right common carotid artery. To record the skin temperature (T_{skin}), we put a plate type of thermoelectric couple (PTP-50; Unique Medical) on the surface of the tail, which was left exposed to room temperature. These two sensors were connected to a custom-made two-channel thermometer. The overall accuracy of repeated measurements in the range of 32–42°C was ±0.01°C. After all the incisions were closed in layers, the rat remained to be laid on a temperature-controlled heating pad (TR-100; Fine Science Tools, North Vancouver, Canada) in a prone position during data recording. The surface of the pad was continuously kept at 37±0.1°C.

Data recording. After the baseline SAP and T_{core} became stable, we altered carotid-sinus baroreceptor pressure (BRP) sequentially in 20 mmHg step increments from 60 to 180 mmHg, then in 20-mmHg decrements from 180 to 60 by the servocontrolled pump. Each step was maintained for 2 minutes. The command signal to the pump was generated by a dedi-

cated laboratory computer (PC-9801RA21; NEC, Tokyo, Japan) through a digital-to-analog converter (DA12-4-98; Contec, Osaka, Japan). The same cycle of sequential changes in BRP was repeated four times over 100 min.

To clarify whether the arterial baroreflex control of T_{core} and T_{skin} was mediated through sympathetic efferents, we examined the effect of bretylium tosylate (12 mg kg^{-1}, I.V.) or hexamethonium (30 mg kg^{-1}, I.V.).

The electrical signals of BRP, SAP, heart rate (HR), T_{core}, and T_{skin} were first low-pass filtered with antialiasing filters having a cutoff frequency of 100 Hz and an attenuation slope of −80 dB/decade (ASIP-0260L; Canopus, Kobe, Japan), then digitized at a rate of 200 Hz by means of an analog-to-digital converter (AD12−16D-98H; Contec).

Data analysis. A preliminary study indicated that the responses of SAP, HR, T_{core}, and T_{skin} to each pressure step imposed on bilateral carotid sinus baroreceptors reached a steady state within 30 s (unpublished observation). Each steady-state value of the responses, therefore, was obtained by an averaging of the latter 30-s values during each pressure step of BRP. Finally, the responses of SAP, HR, T_{core}, and T_{skin} to the same level of BRP in several cycles were averaged for each rat.

The relationship between T_{core} and T_{skin} during sequential changes in BRP was examined by a linear regression analysis.

To parametrically characterize the relationship between the input and output, we analyzed the data with a four-parameter logistic equation model [27]:

$$y=p_4+p_1/[1+\exp\{p_2(x-p_3)\}]$$

where y is the output and x is the input. The four parameters are defined as follows: p_1, the range of change in y (i.e., maximum−minimum values of y); p_2, the coefficient for a calculation of gain; p_3, the value of x corresponding to the midpoint over the range of y; and p_4, the minimum value of y. The instantaneous gain was also calculated from the first derivative of the logistic function, and the maximum gain is $-p_1p_2/4$ at $x=p_3$.

The differences in paired measurements under two conditions were tested by paired t-tests. They were considered significant at $p<0.05$. The values are expressed as means±SD.

RESULTS

A representative example of the original tracings of BRP, SAP, HR, T_{core}, and T_{skin} during 4 cycles of sequential changes in BRP from 60 to 180 mmHg and back again is shown in Fig. 1. Each response of SAP, HR, T_{core}, and T_{skin} to a given input appears to be reproducible during the whole recording procedure. A representative relationship between T_{core} and T_{skin} during a cycle of the sequential changes in BRP from 60 to 180 mmHg and back again is shown in Fig. 2. Although T_{core} was inversely correlated with T_{skin}, the trajectory of the $T_{core}-T_{skin}$ point displayed a hystere-

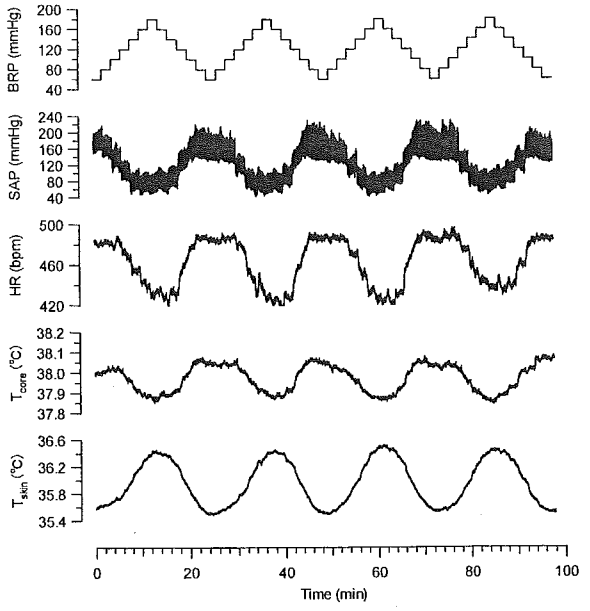

Fig. 1. Original tracings of carotid-sinus baroreceptor pressure (BRP), systemic artery pressure (SAP), heart rate (HR), core temperature (T_{core}), and skin temperature (T_{skin}) during 4 cycles of sequential changes in BRP from 60 to 180 mmHg and back again. The responses of SAP, HR, T_{core}, and T_{skin} to a given input appeared to be consistent throughout the whole recording period.

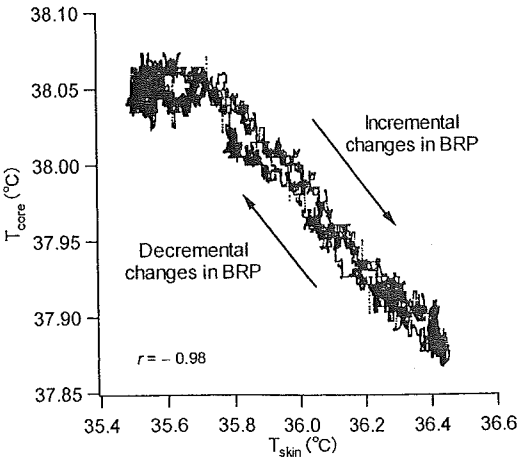

Fig. 2. Graph showing the relationship between core (T_{core}) and skin temperatures (T_{skin}) during a cycle of the sequential changes in carotid-sinus baroreceptor pressure from 60 to 180 mmHg and back again. r, correlation coefficient. See text for details.

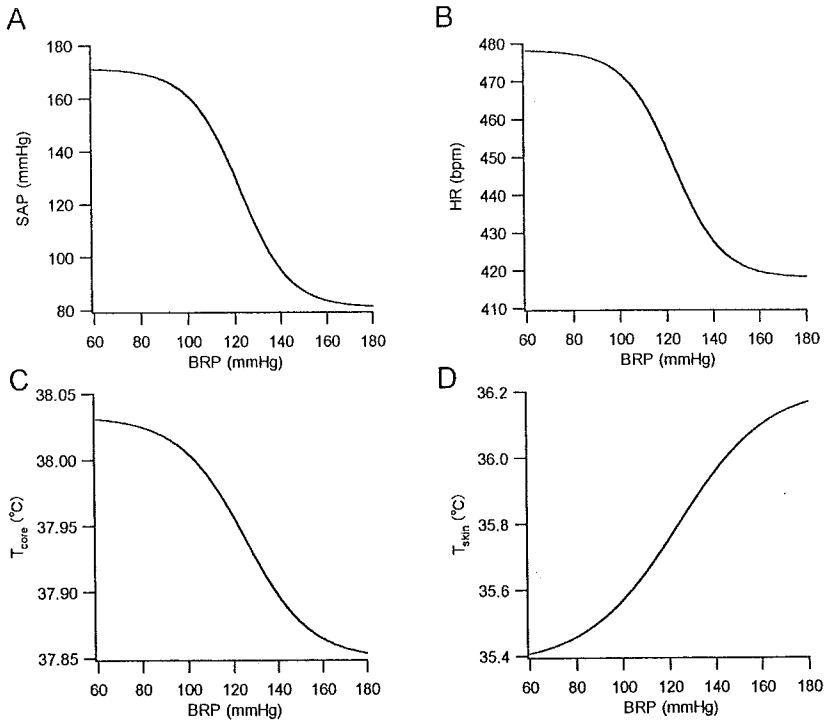

Fig. 3. Graphs showing the relationship of systemic arterial pressure (SAP, A), heart rate (HR, B), core temperature (T_{core}, C), and skin temperature (T_{skin}, D) against carotid-sinus baroreceptor pressure (BRP). Each curve was constructed with the mean values of the parameters of the logistic regression analysis shown in Table 1. See text for details.

Table 1. Four-parameter logistic regression analysis of the relationships of SAP, HR, T_{core}, and T_{skin} against BRP.

	SAP	HR	T_{core}	T_{skin}
p_1	90.3±5.1 mmHg	60.3±10.5 beats min^{-1}	0.18±0.01°C	0.84±0.10°C
p_2	0.093±0.013 mmHg^{-1}	0.095±0.010 mmHg^{-1}	0.069±0.005 mmHg^{-1}	−0.051±0.012 mmHg^{-1}
p_3	122.1±1.6 mmHg	122.7±2.4 mmHg	125.0±1.4 mmHg	123.5±2.9 mmHg
p_4	81.1±7.4 mmHg	418.8±16.5 beats min^{-1}	37.85±0.23°C	35.38±1.08°C

See the METHODS section for the definition of parameters p_1–p_4. SAP, systemic arterial pressure; HR, heart rate; T_{core}, core temperature; T_{skin}, skin temperature; BRP, and carotid-sinus baroreceptor pressure. Values are means±SD for 8 rats.

sis loop. During the incremental change in BRP, the decremental change in T_{core} was preceded by the incremental change in T_{skin}. These characteristics were observed for all the data. The correlation coefficient was −0.97±0.01 for 8 rats. The results of the four-parameter logistic regression analysis of the carotid sinus baroreflex control of SAP, HR, T_{core}, and T_{skin} from 8 rats are summarized in Table 1. In response to the incremental change in BRP by 120 mmHg, SAP, HR, and T_{core} fell by 90.3±5.1 mmHg, 60.3±10.5 beats/min, and 0.18±0.01°C, respectively, but T_{skin} rose by 0.84±0.10°C. The maximum rates of change per unit BRP change were −2.1±0.2 for SAP, −1.5±0.4 beats min^{-1} mmHg^{-1} for HR, −0.003±0.0005°C mmHg^{-1} for T_{core}, and 0.01±0.002°C mmHg^{-1} for T_{skin}. The values of p_3 were 122.1±1.6 mmHg for SAP, 122.7±2.5 mmHg for HR, 125.0±1.4 mmHg for T_{core}, and 123.5±3.0 mmHg for T_{skin}. There was no significant difference in p_3 among them. We then constructed the averaged curves of the sigmoid responses of SAP, HR, T_{core}, and T_{skin} to the BRP (Fig. 3) from mean values for parameters p_1–p_4 shown in Table 1.

After the administration of bretylium or hexamethonium, the baroreflex modulation of T_{core} and T_{skin} was completely abolished (Fig. 4).

DISCUSSION

The present study showed that the baroreflex open-loop analysis yields BRP–T_{core} and BRP–T_{skin} curves with sigmoid shapes. In response to incremental changes in carotid sinus BRP, T_{core} decreased, but T_{skin} increased. The maximum gains of the carotid sinus baroreflex control of SAP, HR, T_{core}, and T_{skin} occurred at the similar level of BRP in normothermic environments.

Baroreflexogenic changes in T_{core} and T_{skin}. The flow of blood to the skin is the most effective mechanism for heat transfer from the body core to the

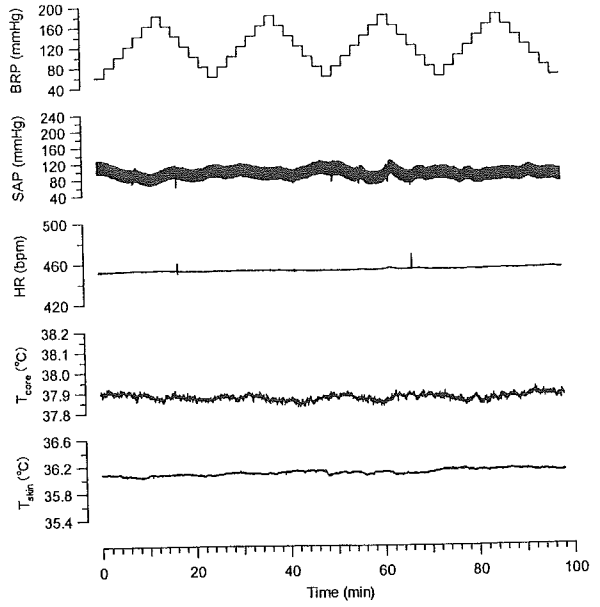

Fig. 4. Original tracings of carotid-sinus baroreceptor pressure (BRP), systemic artery pressure (SAP), heart rate (HR), core temperature (T_{core}), and skin temperature (T_{skin}) during 4 cycles of sequential changes in BRP from 60 to 180 mmHg and back again after the administration of bretylium tosylate (12 mg kg^{-1}, I.V.).

skin. An increase in the skin blood flow causes both a decrease in T_{core} and an increase in T_{skin}. The vasculature of human and nonhuman skins responds to various regulatory reflexes, including those of thermoregulatory and baroreceptor origins [2, 3]. Previous reports suggested that the response of cutaneous circulation to the baroreflex was attributed to cardiopulmonary baroreceptors in humans [3, 15, 16]. In our study, to exclude the participation of the low-pressure baroreceptors of cardiopulmonary regions and to investigate the effect of the arterial baroreceptor on T_{skin}, we cut both vagal nerves and imposed pressure perturbations only on arterial baroreceptors in carotid sinuses. Our results clearly indicated the significant effect of the arterial baroreflex on T_{skin}; the increase in arterial BRP caused the increase in T_{skin}. Thus the arterial baroreceptor reflex is believedto participate in the regulation of cutaneous vasculature. The inverse relationship between T_{core} and T_{skin} reflected the significant role of the blood flow to the skin in the regulation of body temperature. To our knowledge, this is the first report to demonstrate that both T_{core} and T_{skin} are affected by the arterial baroreceptor reflex.

The baroreflex control of the sympathoadrenal system could affect T_{core} and T_{skin} through chemical thermogenesis. However, it is reported that the change in body temperature appeared 2–3 min after the chemical thermogenesis [28]; on the other hand, our data showed that the response of body temperature to a given level of BRP more rapidly reached its steady state within 1–2 min. The inverse relationship between T_{core} and T_{skin} would support the mechanism of heat transfer from the core to the surface rather than the chemical thermogenesis mechanism. From the result that hexamethonium or bretylium diminished the baroreflexogenic change, the major pathway of its efferent limb of the reflex is believed to be the sympathetic nervous system.

Open-loop approach. If arterial pressure is elevated by an external perturbation, the neurogenic vasoconstrictor activity is decreased by the arterial baroreflex. Thereafter T_{skin} increases and T_{core} decreases because of the increase in skin blood flow. This decrease in T_{core} would be sensed by central thermoreceptors [29, 30], and the thermoregulatory center would command the suppression of the skin vasodilatation. Thus the response of T_{skin} to the change in arterial BRP should be attenuated while the central thermoregulatory reflex is functioning. The baroreflexogenic change in T_{skin}, therefore, could be underestimated. These aspects indicate difficulty in the quantitative evaluation of the interaction of the physiological feedback systems under closed-loop conditions. In the present study, we could make an open-loop analysis of the effect of the baroreflex on T_{core} and T_{skin}, and the thermoreflex loop remained closed.

Earlier studies investigated the effect of the arterial baroreflex on body temperatures under the closed-loop conditions of the arterial baroreflex [18–20]. However, vasoactive agents used in these studies for loading or unloading the arterial baroreceptors could directly, i.e., not mediated by the arterial baroreflex, affect the distribution of cardiac output. Thus our approach would be more suitable for clarifying the effect of the arterial baroreflex on body temperatures.

In conclusion, we examined the effect of the arterial baroreflex on core and skin temperatures in halothane-anesthetized rats. To open the baroreflex loop and control BRP, we isolated carotid sinuses. We sequentially altered BRP from 60 to 180 mmHg while measuring SAP, HR, T_{core}, and T_{skin}. In response to the incremental BRP change, SAP, HR, and T_{core} fell, but T_{skin} rose. After the administration of hexamethonium or bretylium, these baroreflexogenic responses were completely abolished. We concluded that T_{core} and T_{skin} are modulated by the arterial baroreceptor reflex.

This study was supported by research grants from Uehara Memorial Foundation, Suzuken Memorial Foundation, Tateisi Science and Technology Foundation, and Mochida Memorial Foundation.

REFERENCES

1. Fox RH and Edholm OG: Nervous control of the cutaneous circulation. Br Med Bull 19: 110–114, 1963
2. Rowell LB: Reflex control of the cutaneous vasculature. J Invest Dermatol 69: 154–166, 1977
3. Johnson JM, Brengelmann GL, Hales JRS, Vanhoutte PM, and Wenger CB: Regulation of the cutaneous circulation. Fed Proc 45: 2841–2850, 1986
4. Wallin BG, Sundolf G, and Delius W: The effect of carotid sinus nerve stimulation on muscle and skin sympathetic nerve activity in man. Pflügers Arch 358: 101–110, 1975
5. Wilson TE, Cui J, and Crandall CG: Absence of arterial baroreflex modulation of skin sympathetic activity and sweat rate during whole-body heating in humans. J Physiol (Lond) 536: 615–623, 2001
6. Crandall CG, Johnson JM, Kosiba WA, and Kellogg DL Jr: Baroreceptor control of the cutaneous active vasodilator system. J Appl Physiol 81: 2192–2198, 1996
7. Wang P, Ba ZF, Burkhardt J, and Chaudry IH: Trauma-hemorrhage and resuscitation in the mouse: effects on cardiac output and organ blood flow. Am J Physiol 264: H1164–H1173, 1993
8. Sapirstein LA, Sapirstein EH, and Bredemeyer A: Effect of hemorrhage on the cardiac output and its distribution in the rat. Circ Res 8: 135–148, 1960
9. Takacs L, Kallay K, and Skolnik JH: Effect of tourniquet shock and acute hemorrhage in the circulation of various organs in the rat. Circ Res 10: 753–757, 1962
10. Pang CCY: Effects of vasopressin antagonist and saralasin in regional blood flow following hemorrhage. Am J Physiol 245: H749–H755, 1983
11. O'Leary DS and Johnson JM: Baroreflex control of the rat tail circulation in normothermia and hyperthermia. J Appl Physiol 66: 1234–1241, 1989
12. Neutze JM, Wyler F, and Rudolph AM: Changes in distribution of cardiac output after hemorrhage in rabbits. Am J Physiol 215: 857–864, 1968
13. Ryan KL, Fred Taylor W, and Bishop VS: Arterial Baroreflex modulation of heat-induced vasodilation in the rabbit ear. J Appl Physiol 83: 2091–2097, 1997.
14. Bond RF, Lackey GF, Taxis JA, and Green HD: Factors governing cutaneous vasoconstriction during hemorrhage. Am J Physiol 219: 1210–1215, 1970
15. Abboud FM, Eckerberg DL, Johannsen UT, and Mark AL: Carotid and cardiopulmonary baroreceptor control of splanchnic and forearm vascular resistance during venous pooling in man. J Physiol (Lond) 286: 173–184, 1979
16. Tripathi A and Nadel ER: Forearm skin and muscle vasoconstriction during lower body negative pressure. J Appl Physiol 60: 1535–1541, 1986
17. Kellogg DL Jr, Johnson JM, and Kostra WA: Baroreflex control of the cutaneous active vasodilator system in humans. Circ Res 66: 1420–1426, 1990
18. Shibata H: Baroreflex suppression of nonshivering thermogenesis in rats. Jpn J Physiol 32: 937–944, 1982
19. Nunomura T, Nagasaka T, and Shibata H: Effects of restraint on baroreflex sensitivity in altering heart rate and heat production in rats. Jpn J Physiol 33: 667–670, 1983
20. Shido O and Nagasaka T: Effects of intraventricular neurotensin on blood pressure and heat balance in rats. Jpn J Physiol 35: 311–320, 1985
21. Sato T, Kawada T, Inagaki M, Shishido T, Sugimachi M, and Sunagawa K: Dynamics of sympathetic baroreflex control of arterial pressure in rats. Am J Physiol 285: R262–R270, 2003
22. Sato T, Kawada T, Inagaki M, Shishido T, Takaki H, Sugimachi M, and Sunagawa K: New analytic framework for understanding sympathetic baroreflex control of arterial pressure. Am J Physiol 276: H2251–H2261, 1999
23. Sato T, Kawada T, Miyano H, Shishido T, Inagaki M, Yoshimura R, Tatewaki T, Sugimachi M, Alexander J Jr, and Sunagawa K: New simple methods for isolating baroreceptor regions of carotid sinus and aortic depressor nerves in rats. Am J Physiol 276: H326–H332, 1999
24. Sato T, Kawada T, Sugimachi M, and Sunagawa K: Bionic technology revitalizes native baroreflex function in rats with baroreflex failure. Circulation 106: 730–734, 2002
25. Ono A, Kuwaki T, Kumada M, and Fujita T: Differential central modulation of the baroreflex by salt loading in normotensive and spontaneously hypertensive rats. Hypertension 29: 808–814, 1997
26. Dibona GF and Sawin LL: Reflex regulation of renal nerve activity in cardiac failure. Am J Physiol 226: R27–R39, 1994
27. Kent BB, Drane JW, Blumenstein B, and Manning JW: A mathematical model to assess changes in the baroreceptor reflex. Cardiology 57: 295–310, 1972
28. Nedergaard J and Lindberg O: The brown fat cell. Int Rev Cytol 74: 187–286, 1982
29. Wyss CR, Brengelmann GL, Johnson JM, Rowell LB, and Silverstein D: Altered control of skin blood flow at high skin and core temperatures. J Appl Physiol 38: 839–845, 1975
30. Nakajima Y, Mizobe T, Takamata A, and Tanaka Y: Baroreflex modulation of peripheral vasoconstriction during progressive hypothermia in anesthetized humans. Am J Physiol 279: R1430–R1436, 2000

Vagal Nerve Stimulation Markedly Improves Long-Term Survival After Chronic Heart Failure in Rats

Meihua Li, MS; Can Zheng, PhD; Takayuki Sato, MD; Toru Kawada, MD; Masaru Sugimachi, MD; Kenji Sunagawa, MD

Background—Diminished cardiac vagal activity and higher heart rate predict a high mortality rate of chronic heart failure (CHF) after myocardial infarction. We investigated the effects of chronic electrical stimulation of the vagus nerve on cardiac remodeling and long-term survival in an animal model of CHF after large myocardial infarction.

Methods and Results—Two weeks after the ligation of the left coronary artery, surviving rats were randomized to vagal- and sham-stimulated groups. Using an implantable miniature radio-controlled electrical stimulator, we stimulated the right vagal nerve of CHF rats for 6 weeks. The intensity of electrical stimulation was adjusted for each rat, so that the heart rate was lowered by 20 to 30 beats per minute. The treated rats had significantly lower left ventricular end-diastolic pressure (17.1±5.9 versus 23.5±4.2 mm Hg, $P<0.05$) and higher maximum dp/dt of left ventricular pressure (4152±237 versus 2987±192 mm Hg/s, $P<0.05$) than the untreated rats. Improvement of cardiac pumping function was accompanied by a decrease in normalized biventricular weight (2.75±0.25 versus 3.14±0.22 g/kg, $P<0.01$). Although the 140-day survival of the untreated group was only half, vagal stimulation markedly improved the survival rate (86% versus 50%, $P=0.008$). Vagal stimulation therapy achieved a 73% reduction in a relative risk ratio of death.

Conclusions—Vagal nerve stimulation markedly improved the long-term survival of CHF rats through the prevention of pumping failure and cardiac remodeling. (***Circulation.* 2004;109:120-124.**)

Key Words: electrical stimulation ■ heart failure ■ myocardial infarction ■ remodeling ■ vagus nerve

Acute myocardial infarction[1] occurs when blood supply to part of the heart muscle is severely reduced or stopped. Survivors after large myocardial infarction have a high risk for chronic heart failure (CHF), with poor prognosis. CHF is a clinical syndrome that is initiated by cardiac dysfunction and followed by activation of compensatory mechanisms such as the sympathoadrenal and renin-angiotensin-aldosterone systems. Apparently, activation of compensatory mechanisms during the early phase of CHF helps the heart compensate for deteriorating pumping function. However, excessive sustained activation has deleterious effects on cardiac function. Once such an excessive activation, on the contrary, worsens cardiac function, it triggers further activation of those compensatory mechanisms, which, in turn, further deteriorates cardiac function. This positive feedback mechanism leads the heart to decompensatory cardiac remodeling and failure at the end stage. Therefore, the maladaptation process is a key of pathophysiology of CHF.

In the maladaptation process, the cardiac autonomic nervous system[2,3] also plays an important role. Clinical evidence from the Autonomic Tone and Reflexes After Myocardial Infarction study (ATRAMI)[4] and the Cardiac Insufficiency BIsoprolol Study II (CIBIS II)[5] indicates that diminished cardiac vagal activity and increased heart rate predict a high mortality rate of CHF. Based on this body of knowledge, it would be logical to clarify whether augmentation of vagal activity prevents cardiac remodeling and death. On the occurrence of life-threatening arrhythmias in acute ischemia, the effect of vagal stimulation has been reported to prevent ventricular fibrillation in dogs.[6] The antianginal effect of vagal stimulation has been also shown in patients with coronary artery disease.[7] However, its effect on CHF remains unknown. Therefore, in the present study, we examined the effects of vagal stimulation on cardiac remodeling after large myocardial infarction and on the long-term prognosis of CHF in rats.

Methods

Experimental Heart Failure

The care and use of the animals were in strict accordance with the guiding principles of the Physiological Society of Japan. Left ventricular myocardial infarction was induced by coronary artery ligation in 8-week-old male Sprague-Dawley rats (SLC, Hamamatsu, Japan). The mortality rate in animals with myocardial infarction was ≈60% within the first 24 hours. One week later, we checked the infarct size by echocardiography (SSA-380A, Toshiba), as described previously.[8] The rats with infarcted area >40% of the left ventricular

Received January 16, 2003; de novo received June 4, 2003; revision received August 25, 2003; accepted August 26, 2003.

From the Department of Cardiovascular Dynamics, National Cardiovascular Center Research Institute, Suita, Japan (M.L., C.Z., T.S., T.K., M.S., K.S.); and the Department of Cardiovascular Control, Kochi Medical School, Nankoku, Japan (T.S.).

Correspondence to Takayuki Sato, MD, Department of Cardiovascular Control, Kochi Medical School, Nankoku, Kochi 783-8505, Japan. E-mail tacsato-kochimed@umin.ac.jp

Circulation is available at http://www.circulationaha.org

DOI: 10.1161/01.CIR.0000105721.71640.DA

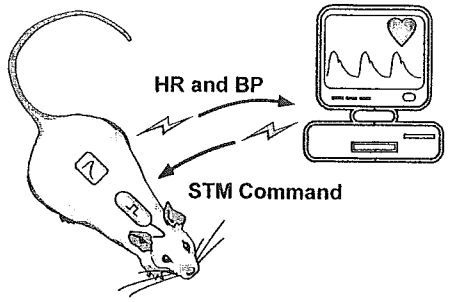

Figure 1. Neural interface approach to stimulate the vagal nerve. While monitoring heart rate through an implantable transmitter, a remote control system adjusted the intensity of electrical pulses of an implantable miniature radio-controlled electrical stimulator.

wall were enrolled in the present study. In sham-operated rats, we loosely tied a suture to avoid coronary artery occlusion. We confirmed the infarct size by postmortem examination.

Vagal Nerve Stimulation

To stimulate the vagal nerve and to monitor blood pressure and heart rate in freely moving rats, we developed a remote system controlled by a computer (Figure 1). The computer commands an implantable and radio-controlled pulse generator (ISE1010C, Unimec) to stimulate the vagal nerve while sensing blood pressure and heart rate through an implantable transmitter (TA11PA-C40, Data Sciences International). The miniature pulse generator and transmitter were subcutaneously implanted in the abdomen at 7 days after myocardial infarction. A pair of Teflon-coated stainless steel wires for electrical stimulation was looped around the right vagal nerve in the neck; a Teflon tube for blood pressure recording was placed in the abdominal aorta.

Experimental Protocols

At 14 days after myocardial infarction, the survivors were randomized into groups treated with sham and active stimulation. In the actively treated group, we stimulated the vagal nerve with electrical rectangular pulses of 0.2-ms duration at 20 Hz for 10 seconds every minute for 6 weeks. The electrical current of pulses was adjusted for each rat, so that the heart rate was lowered by 20 to 30 beats per minute. This resulted in the ranges of 0.1 to 0.13 mA. Mean blood pressure and heart rate were recorded every minute for 6 weeks. In a preliminary study, we confirmed that the chronic vagal stimulation at this intensity did not alter feeding behavior and did not evoke any signs of pain reaction such as an increase in plasma epinephrine level.

Hemodynamic and Remodeling Study

To evaluate the effect of vagal stimulation on cardiac remodeling, at the end of the 6-week stimulation period we measured hemodynamics and heart weights of sham-operated and sham-stimulated rats, untreated CHF rats, and treated CHF rats. Anesthesia was maintained through the use of 1.2% halothane during surgical procedures and 0.6% halothane during data recording. Left ventricular and arterial pressures were measured with a 2F catheter-tipped micromanometer (SPC-320, Millar Instruments). Pressure signals were digitized at a rate of 1 kHz for 5 minutes. After hemodynamic measurement, the heart was excised for subsequent determination of infarct size.

Prognosis and Neurohormone Study

To examine the effect of 6-week vagal stimulation on prognosis, we observed a 20-week survival rate in treated and untreated CHF rats. Because of the life of the battery of the implantable pulse generator, the treatment period was limited to 6 weeks. Each cage was inspected daily for the rat that had died. The heart was removed from the dead animal for subsequent determination of infarct size.

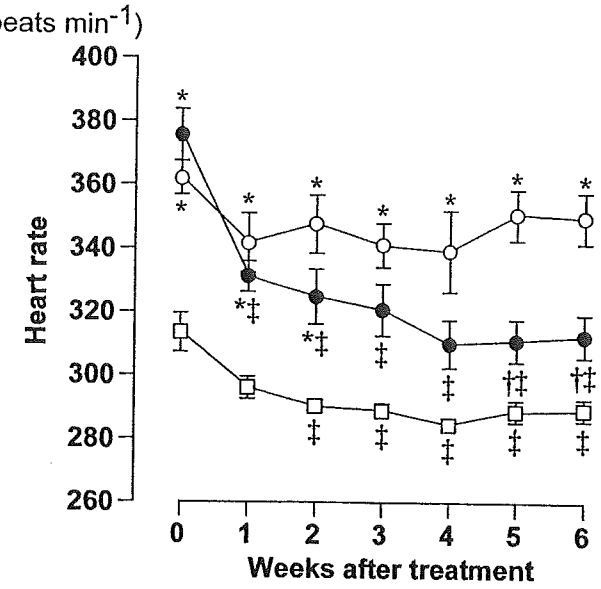

Figure 2. Effects of 6-week vagal nerve stimulation on 24-hour average of heart rate of sham-operated (SO-SS, □, n=9) rats treated with sham stimulation, CHF rats treated with sham (CHF-SS, ○, n=13), and vagal stimulation (CHF-VS, ●, n=11). Data are expressed as mean±SEM. *P<0.05 from SO-SS group; †P<0.05 from CHF-SS group; ‡P<0.05 from pretreatment values of each group.

At the end of the observation period, blood for neurohormone assays was sampled. The surviving rat was placed in a glass jar, where it inspired a mixture of 1.2% halothane in oxygen-enriched air for 5 to 10 minutes. To avoid the modification of neurohumoral states by invasive manipulation, immediately after the induction of anesthesia, we quickly collected 3 mL of a blood sample from the left ventricular cavity through a transthoracic approach without measuring hemodynamics. After blood sampling, the heart was excised for subsequent determination of infarct size.

Plasma concentrations of norepinephrine were measured by high-performance liquid chromatography with electrochemical detection. Plasma levels of brain natriuretic peptide were determined by radioimmunoassay.

Determination of Infarct Size

As described previously,[9] the right ventricle and the left ventricle including the interventricular septum were dissected, separated, and weighted. The heart was fixed in 10% buffered formalin. The left ventricle was cut from apex to base into 4 transverse slices. Sections 4 μm thick were cut and stained by Masson trichrome method. Histological images were digitized through a frame grabber and analyzed. Infarct size was calculated from the 4 slices by dividing the sum of the endocardial lengths of infarcted regions by the sum of the total endocardial circumferences.

Statistical Analysis

For data of the hemodynamic and remodeling study, differences among 3 groups were tested by ANOVA, with a Scheffé multiple comparison test. Differences in heart rates before and during treatment in each group were examined by a 1-way ANOVA with repeated measures, followed by a post hoc Dunnett test.

For a neurohormonal data, differences between two groups were examined by a Mann-Whitney U test. Survival data are presented as Kaplan-Meier curves; the effect of treatment on 140-day survival was analyzed by a Fisher exact test. Differences were considered significant at a value of P<0.05.

Mean Blood Pressure (mm Hg)

		Weeks After Stimulation					
Group	Before	1	2	3	4	5	6
SO-SS	104±2	104±3	104±3	103±3	102±3	102±2	104±3
CHF-SS	83±3*	83±6*	83±6*	83±9*	85±9*	83±7*	81±6*
CHF-VS	85±10*	82±5*	82±7*	81±7*	80±7*	82±6*	83±7*

SO-SS indicates sham-operated rats treated with sham stimulation (SS); CHF-SS, CHF rats treated with sham stimulation; CHF-VS, CHF rats treated with vagal stimulation. Values are mean±SD of the 24-hour average of mean blood pressure.

*$P<0.01$ from SO-SS group.

Results

Hemodynamic and Remodeling Study

Although CHF rats (untreated, n=13; treated, n=11) had a higher heart rate than sham-operated rats (n=9) before the treatment, vagal stimulation significantly slowed the heart rate of CHF rats (Figure 2). The difference in heart rate between untreated and treated CHF rats reached ≈40 beats per minute at the end of treatment ($P<0.05$). CHF rats had significantly lower blood pressure, but the vagal stimulation did not affect blood pressure during the 6-week treatment period (Table).

When compared with sham-operated rats, untreated CHF rats had low blood pressure (Figure 3a), high left ventricular end-diastolic pressure (LVEDP) (Figure 3b), a depressed maximum dp/dt of left ventricular pressure ($LV+dp/dt_{max}$) (Figure 3c), and an increased heart weight (Figure 3d). On the other hand, CHF rats treated with vagal nerve stimulation had significantly lower LVEDP (17.1±5.9 versus 23.5±4.2 mm Hg, $P<0.05$) and higher $LV+dp/dt_{max}$ (4152±237 versus 2987±192 mm Hg/s, $P<0.05$) than untreated CHF rats. Improvement of pumping function in treated CHF rats was accompanied by a significant decrease in normalized biventricular weight (2.75±0.25 versus 3.14±0.22 g/kg, $P<0.01$). There was no significant difference in infarct size between treated and untreated CHF rats (53±7% versus 53±6%).

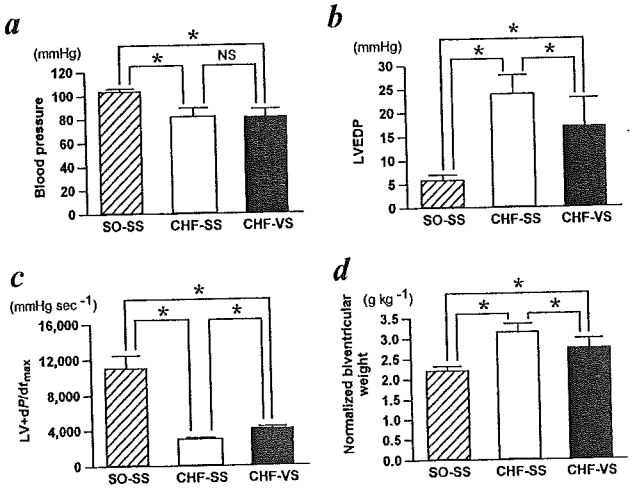

Figure 3. Effects of vagal nerve stimulation on a, mean blood pressure; b, LVEDP; c, maximum dp/dt of left ventricular pressure ($LV+dP/dt_{max}$); d, biventricular weight normalized by body weight in sham-operated (SO-SS, hatched bar, n=9) rats treated with sham stimulation, CHF rats treated with sham (CHF-SS, open bar, n=13), and vagal stimulation (CHF-VS, closed bar, n=11). Assessment was made at the end of 6-week treatment. Data are expressed as mean±SD. *$P<0.05$; ‡$P<0.01$.

Prognosis and Neurohormone Study

Although 60 rats with CHF after large myocardial infarction were enrolled in the prognosis study, 8 of the 30 rats assigned to the treated group were excluded from the results because of the breaking down of electrode wires during vagal stimulation for 6 weeks. Vagal nerve stimulation markedly suppressed the mortality rate of CHF rats (Figure 4); there were only 3 deaths among the 22 treated rats versus 15 deaths among the 30 untreated rats (14% versus 50%, $P=0.008$). Vagal stimulation therapy achieved a 73% reduction in a relative risk ratio of death.

Shown in Figure 5, improvement of survival in treated CHF rats was accompanied by a significant decrease in normalized biventricular weight (2.63±0.38 versus 3.17±0.42 g/kg, $P<0.01$). When compared with untreated CHF rats, treated CHF rats had lower levels of plasma norepinephrine (426±102 versus 1182±260 pg/mL, $P<0.01$) and brain natriuretic peptide (251±31 versus 363±82 pg/mL, $P<0.01$). There was no significant difference in infarct size between treated and untreated CHF rats (54±8% versus 53±7%).

Discussion

The prognosis of patients with CHF is still poor, even though various therapeutic approaches with a β-adrenergic receptor

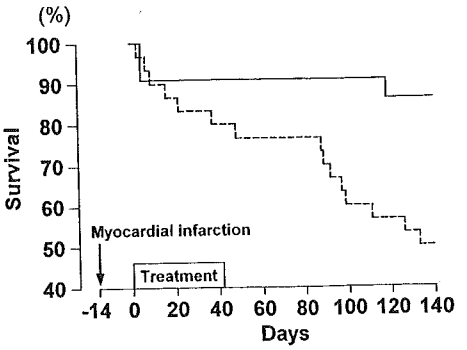

Figure 4. Effects of vagal nerve stimulation on survival curves of CHF rats treated with sham (broken line, n=30) and vagal stimulation (solid line, n=22). Treatment started 14 days after coronary artery ligation. Vagal stimulation significantly ($P=0.008$) improved survival rate.

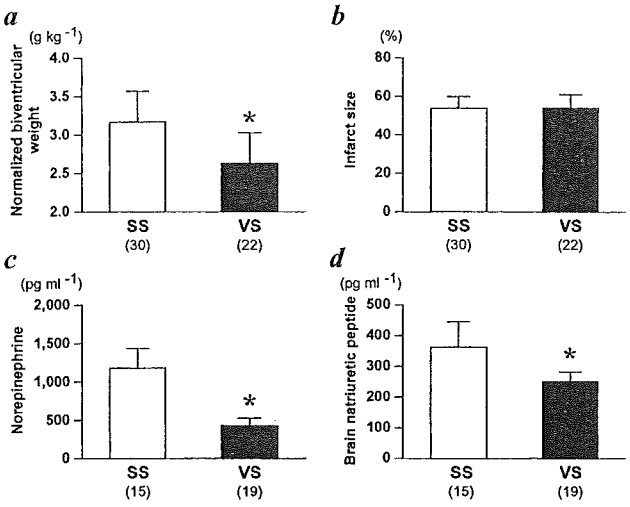

Figure 5. Comparison of biventricular weight normalized by body weight (a), infarct size (b), and plasma levels of norepinephrine (c) and brain natriuretic peptide (d) in CHF rats treated with sham stimulation (SS) and vagal stimulation (VS). Each value in parentheses indicates number of animals in each group. *$P<0.01$.

blocker,[10,11] angiotensin-converting enzyme inhibitor,[12] angiotensin-receptor blocker,[13] aldosterone antagonist,[14] and implantable defibrillator[15] are currently available. Therefore, more effective modality of therapy is expected.

The present results indicate that vagal nerve stimulation markedly improved the long-term survival of CHF rats through prevention of the progression of pumping failure and cardiac remodeling. The main objective of the present study was to test the working hypothesis that long-term vagal stimulation can improve survival of CHF rats after large myocardial infarction, not to clarify the mechanism. However, some considerations on this issue are warranted.

It is conceivable that vagal stimulation may effectively sever the vicious cycle leading to death through an inhibitory effect on presynaptic norepinephrine releases and suppressive effects on adrenergic signaling cascade through G-protein interactions.[16] In human hearts as well as those of several other species, muscarinic receptors are predominantly of the M_2-subtype, which couples through a pertussis toxin–sensitive G_i protein to inhibit adenyl cyclase. In the atrium, stimulation of muscarinic M_2 receptors causes direct negative inotropic and chronotropic effects; in the ventricle, on the other hand, the negative inotropic effect can be only achieved when the basal level of cAMP is elevated by β-adrenoceptor agonists. These mechanisms are known as accentuated antagonism.

Vagal stimulation is also postulated to improve ventricular efficiency by slowing heart rate.[17] Burkhoff et al[18] showed that the ventricular efficiency, that is, the ratio of ventricular stroke work to ventricular oxygen consumption, is adjusted to be maximal under physiological conditions and that the efficiency of the failing heart is more sensitive to changes in heart rate than that of the normal heart. Prevention of tachycardia after myocardial infarction by vagal stimulation would optimize the efficiency of the failing heart and thus protect the heart against remodeling.

Apparently, vagal efferent stimulation is considered to act on the ventricle of CHF like a β-adrenergic blocker. However, in rats, β-blockade therapy rather failed to exert a beneficial effect on the cardiac remodeling or hemodynamics after myocardial infarction (for review, see Gaballa and Goldman[19]). Litwin et al[20] showed that chronic propranolol treatment did not improve cardiac remodeling and worsened pumping function in rats with postinfarction CHF. Wei et al[21] also demonstrated that metoprolol deteriorated ventricular remodeling in CHF rats. Therefore, in addition to antagonism against sympathetic effects, unique actions of vagal stimulation would be important in providing the favorable outcome for CHF rats. A facilitatory effect of vagal stimulation on nitric oxide release from the coronary endothelium could also have an antiremodeling action through improvement of viable myocardial conditions.[22]

In addition to the effects of electrical stimulation of vagal efferents on the heart, vagal afferent effects[7,23] are also considered because afferent stimulation would evoke cardiopulmonary reflex and modulate neuronal activity in several hypothalamic nuclei involved in cardiovascular regulation. As shown in Figure 5c, vagal stimulation lowered the plasma norepinephrine level. Therefore, vagal stimulation therapy would terminate the vicious circle of maladaptation in CHF through the suppression of chronic excessive activation of the sympathetic nervous system.[24,25]

A more recent study by Guarini et al[26] has shown that efferent vagal fiber stimulation blunts activation of nuclear factor-κB in the liver through nicotinic receptors and then reduces the hepatic production and the plasma level of tumor necrosis factor-α during acute hemorrhagic shock. It has been reported that these factors are also involved in cardiac remodeling and the poor prognosis of CHF.[27] Therefore, the hepatic effect of vagal stimulation would prevent cardiac remodeling and improve survival of CHF.

It is also noted that short-term vagal stimulation for 6 weeks after myocardial infarction prevented long-term cardiac remodeling (Figure 5a) and improved the long-term survival. There may be a critical period during which short-term treatment against cardiac dysfunction and remodeling will ensure the long-term survival of CHF.

A pioneer work by Pfeffer et al[28] examined the effect of long-term therapy with captopril in CHF rats after myocardial infarction. As well as vagal stimulation in the present study, oral captopril administration started at 14 days after ligation of the left coronary artery. Pfeffer et al observed 1-year survival and found that the median survival was 146 and 181 days for untreated and treated CHF rats with large infarcts, respectively. Thus, the survival curve of untreated CHF rats with large infarcts in their study was quite similar to our result of untreated CHF rats. On the other hand, the effect of captopril on survival in CHF rats with large infarcts appeared to be much different from that of vagal stimulation. Approximately 40% of captopril-treated CHF rats with large infarcts died at 140 days; vagal stimulation reduced the mortality rate to <20%. Therefore, vagal stimulation therapy may be promising for severe CHF after large myocardial infarction.

Limitations

The beneficial effects of vagal stimulation on cardiac function, remodeling, and survival of CHF rats were shown in the present study. However, its safety and adverse effects remain to be unclear. The appropriate protocol of treatment is also still unsettled and should be investigated. To establish the therapeutic strategy shown in this study, large-scale, long-term trials of vagal nerve stimulation with an animal model of CHF are required.

Clinical Implications

Our previous studies[9,29] indicated that a pharmacological intervention in the central nervous system of CHF rats prevented the progression of cardiac dysfunction and remodeling. The therapeutic modality used in the present study also brought a favorable prognosis of CHF by manipulation of autonomic tone through vagal efferent and/or afferent mechanisms. We therefore propose the neural interface approach to optimize cardiac autonomic tone for the treatment of CHF. Technologies to materialize this neural interface strategy[30] using totally implantable miniaturized systems are readily available.[31,32]

Acknowledgments

This study was supported by a Health and Labor Sciences Research Grant (H14-NANO-002) for Advanced Medical Technology from the Ministry of Health, Labor, and Welfare of Japan, a Ground-Based Research Grant for the Space Utilization from NASDA and Japan Space Forum, and a Research Grant from Mitsubishi Pharma Research Foundation.

References

1. Pfeffer MA. Left ventricular remodeling after acute myocardial infarction. *Annu Rev Med.* 1995;46:455–466.
2. Cerati D, Schwartz PJ. Single cardiac vagal fiber activity, acute myocardial ischemia, and risk for sudden death. *Circ Res.* 1991;69:1389–1401.
3. Schwartz PJ, La Rovere MT, Vanoli E. Autonomic nervous system and sudden cardiac death: experimental basis and clinical observations for post-myocardial infarction risk stratification. *Circulation.* 1992;85(suppl I):I-77–I-91.
4. La Rovere MT, Bigger JT Jr, Marcus FI, et al. Baroreflex sensitivity and heart-rate variability in prediction of total cardiac mortality after myocardial infarction. *Lancet.* 1998;351:478–484.
5. Lechat P, Hulot JS, Escolano S, et al. Heart rate and cardiac rhythm relationships with bisoprolol benefit in chronic heart failure in CIBIS II trial. *Circulation.* 2001;103:1428–1433.
6. Vanoli E, De Ferrari GM, Stramba-Badiale M, et al. Vagal stimulation and prevention of sudden death in conscious dogs with a healed myocardial infarction. *Circ Res.* 1991;68:1471–1481.
7. Zamotrinsky A, Kondratiev, de Jong JW. Vagal neurostimulation in patients with coronary artery disease. *Auton Neurosci Basic Clin.* 2001;88:109–116.
8. Litwin SE, Katz SE, Morgan JP, et al. Serial echocardiographic assessment of left ventricular geometry and function after large myocardial infarction in the rat. *Circulation.* 1994;89:345–354.
9. Sato T, Yoshimura R, Kawada T, et al. The brain is a possible target for an angiotensin-converting enzyme inhibitor in the treatment of chronic heart failure. *J Card Fail.* 1998;4:139–144.
10. Nagatsu M, Spinale FG, Koide M, et al. Bradycardia and the role of β-blockade in the amelioration of left ventricular dysfunction. *Circulation.* 2000;101:653–659.
11. Packer M, Coats AJ, Fowler MB, et al. Effect of carvedilol on survival in severe heart failure. *N Engl J Med.* 2001;344:1651–1658.
12. Yusuf S, Sleight P, Pogue J, et al. Effects of an angiotensin-converting-enzyme inhibitor, ramipril, on cardiovascular events in high-risk patients. *N Engl J Med.* 2000;342:145–153.
13. Cohn JN, Tognoni GA. Randomized trial of the angiotensin-receptor blocker valsartan in chronic heart failure. *N Engl J Med.* 2001;345:1667–1675.
14. Pitt B, Zannad F, Remme WJ, et al. The effect of spironolactone on morbidity and mortality in patients with severe heart failure. *N Engl J Med.* 1999;341:709–717.
15. Moss AJ, Zareba W, Hall WJ, et al. Prophylactic implantation of a defibrillator in patients with myocardial infarction and reduced ejection fraction. *N Engl J Med.* 2002;346:877–883.
16. Giessler C, Dhein S, Ponicke K, et al. Muscarinic receptors in the failing human heart. *Eur J Pharmacol.* 1999;375:197–202.
17. Schoemaker RG, Saxena PR, Kalkman EAJ. Low-dose aspirin improves in vivo hemodynamics in conscious, chronically infarcted rats. *Cardiovasc Res.* 1998;37:108–114.
18. Burkhoff D, Sagawa K. Ventricular efficiency predicted by an analytic model. *Am J Physiol.* 1986;250:R1021–R1027.
19. Gaballa MA, Goldman S. Ventricular remodeling in heart failure. *J Card Fail.* 2002;8:S476–S485.
20. Litwin SE, Katz SE, Morgan JP, et al. Effects of propranolol treatment on left ventricular function and intracellular calcium regulation in rats with postinfarction heart failure. *Br J Pharmacol.* 1999;127:1671–1679.
21. Wei S, Chow LTC, Sanderson JE. Effect of carvedilol in comparison with metoprolol on myocardial collagen postinfarction. *J Am Coll Cardiol.* 2000;36:276–281.
22. Zhao G, Shen W, Xu X, et al. Selective impairment of vagally mediated, nitric oxide-dependent coronary vasodilation in conscious dogs after pacing-induced heart failure. *Circulation.* 1995;91:2655–2663.
23. Mark AL. Sensitization of cardiac vagal afferent reflexes at the sensory receptor level: an overview. *Fed Proc.* 1987;46:36–40.
24. Swedberg K, Eneroth P, Kjekshus J, et al. Hormones regulating cardiovascular function in patients with severe congestive heart failure and their relation to mortality. *Circulation.* 1990;82:1730–1736.
25. Ceiler DL, Schiffers PMH, Nelissen-Vrancken HJMG, et al. Time-related adaptation in plasma neurohormone levels and hemodynamics after myocardial infarction in the rat. *J Card Fail.* 1998;4:131–138.
26. Guarini S, Altavilla D, Cainazzo, MM, at al. Efferent vagal fiber stimulation blunts nuclear factor-κB activation and protects against hypovolemic hemorrhagic shock. *Circulation.* 2003;107:1189–1194.
27. Mann DL. Tumor necrosis factor-induced signal transduction and left ventricular remodeling. *J Card Fail.* 2002;8:S379–S386.
28. Pfeffer MA, Pfeffer JM, Steinberg C, et al. Survival after an experimental myocardial infarction: beneficial effects of long-term therapy with captopril. *Circulation.* 1985;72:406–412.
29. Yoshimura R, Sato T, Kawada T, et al. Increased brain angiotensin receptor in rats with chronic high-output heart failure. *J Card Fail.* 2000;6:66–72.
30. Sato T, Kawada T, Sugimachi M, et al. Bionic technology revitalizes native baroreflex function in rats with baroreflex failure. *Circulation.* 2002;106:730–734.
31. Reid SA. Surgical technique for implantation of the neurocybernetic prosthesis. *Epilepsia.* 1990;31(suppl 2):S38–S39.
32. Murphy JV, Patil A. Stimulation of the nervous system for the management of seizures: current and future developments. *CNS Drugs.* 2003;17:101–115.

J Appl Physiol 97: 984–990, 2004.
First published May 7, 2004; 10.1152/japplphysiol.00162.2004.

Bionic epidural stimulation restores arterial pressure regulation during orthostasis

Yusuke Yanagiya,[1,2] Takayuki Sato,[1,3] Toru Kawada,[1] Masashi Inagaki,[1] Teiji Tatewaki,[1,4] Can Zheng,[1,2] Atsunori Kamiya,[1] Hiroshi Takaki,[1] Masaru Sugimachi,[1] and Kenji Sunagawa[1]

[1]*Department of Cardiovascular Dynamics, National Cardiovascular Center Research Institute, Suita, Osaka 565-8565;*
[2]*Pharmaceuticals and Medical Devices Agency, Chiyoda-ku, Tokyo 100-0013;*
[3]*Department of Cardiovascular Control, Kochi Medical School, Nankoku, Kochi 783-8505;*
and [4]*Japan Association for the Advancement of Medical Equipment, Bunkyo-ku, Tokyo 113-0033, Japan*

Submitted 13 February 2004; accepted in final form 30 April 2004

Yanagiya, Yusuke, Takayuki Sato, Toru Kawada, Masashi Inagaki, Teiji Tatewaki, Can Zheng, Atsunori Kamiya, Hiroshi Takaki, Masaru Sugimachi, and Kenji Sunagawa. Bionic epidural stimulation restores arterial pressure regulation during orthostasis. *J Appl Physiol* 97: 984–990, 2004. First published May 7, 2004; 10.1152/japplphysiol.00162.2004.—A bionic baroreflex system (BBS) is a computer-assisted intelligent feedback system to control arterial pressure (AP) for the treatment of baroreflex failure. To apply this system clinically, an appropriate efferent neural (sympathetic vasomotor) interface has to be explored. We examined whether the spinal cord is a candidate site for such interface. In six anesthetized and baroreflex-deafferentiated cats, a multielectrode catheter was inserted into the epidural space to deliver epidural spinal cord stimulation (ESCS). Stepwise changes in ESCS rate revealed a linear correlation between ESCS rate and AP for ESCS rates of 2 pulses/s and above (r^2, 0.876–0.979; slope, 14.3 ± 5.8 mmHg·pulses^{-1}·s; pressure axis intercept, 35.7 ± 25.9 mmHg). Random changes in ESCS rate with a white noise sequence revealed dynamic transfer function of peripheral effectors. The transfer function resembled a second-order, low-pass filter with a lag time (gain, 16.7 ± 8.3 mmHg·pulses^{-1}·s; natural frequency, 0.022 ± 0.007 Hz; damping coefficient, 2.40 ± 1.07; lag time, 1.06 ± 0.41 s). On the basis of the transfer function, we designed an artificial vasomotor center to attenuate hypotension. We evaluated the performance of the BBS against hypotension induced by 60° head-up tilt. In the cats with baroreflex failure, head-up tilt dropped AP by 37 ± 5 mmHg in 5 s and 59 ± 11 mmHg in 30 s. BBS with optimized feedback parameters attenuated hypotension to 21 ± 2 mmHg in 5 s ($P < 0.05$) and 8 ± 4 mmHg in 30 s ($P < 0.05$). These results indicate that ESCS-mediated BBS prevents orthostatic hypotension. Because epidural stimulation is a clinically feasible procedure, this BBS can be applied clinically to combat hypotension associated with various pathophysiologies.

baroreceptors; blood pressure; autonomic nervous system; Shy-Drager syndrome; orthostatic hypotension

THE ARTERIAL BAROREFLEX SYSTEM configures a negative feedback system and reduces arterial pressure (AP) disturbances from external influences (9, 15, 22, 23). Sudden onset of hypotension by orthostatic change occurs as a result of baroreflex failure, despite normal functioning of the cardiovascular system and efferent sympathetic nervous system. This condition is seen in multiple-system atrophy (Shy-Drager syndrome) (21, 22, 30) as well as spinal cord injuries (7, 17). Current treatments, such as salt loading (19, 33), cardiac pacing (1, 14), and pharmacological interventions (2, 3, 12, 20), fail to prevent the orthostatic hypotension. These therapies often result in an unwanted increase in AP in the supine position and neither restore nor reproduce the function of the feedback system that forms the basis of AP control (See DISCUSSION).

Previously, our laboratory developed a bionic baroreflex system (BBS) that substitutes the defective vasomotor center with an artificial controller (i.e., an artificial vasomotor center) to restore the native baroreflex function (24, 26). In these animal studies, the celiac ganglion was exposed by laparotomy and stimulated directly as the efferent neural interface in the BBS. However, for clinical application of the BBS, a less invasive and more stable electrical stimulation method is required.

In the present study, we examined the hypothesis that the spinal cord is a candidate site for the efferent neural interface in our bionic strategy. Epidural spinal cord stimulation (ESCS) has been used for the management of patients with malignant neoplasm, angina pectoris, and peripheral ischemia (6, 29). Stimulating the dorsal part of the spinal cord changes sympathetic nerve activity, AP in animals (11, 32) and heart rate in humans (18). If we can delineate how ESCS affects AP quantitatively, then this may lead to clinical application of the BBS. We studied the feasibility of ESCS-mediated BBS using an animal model of central baroreflex failure.

MATERIALS AND METHODS

Study design. BBS is a negative feedback system and consists of two components: peripheral effectors and the artificial vasomotor center (Fig. 1). Peripheral effectors change AP in response to ESCS. The artificial vasomotor center (controller) determines the ESCS rate in response to changes in AP. Using BBS, we computer programmed the artificial vasomotor center and substituted the defective vasomotor center with an artificial vasomotor center.

For this purpose, we first characterized the static as well as dynamic responses of the peripheral effectors. With this knowledge, we then designed an artificial vasomotor center using simulation to delineate the parameters for obtaining optimal AP response. Finally, we evaluated the performance of the ESCS-mediated BBS in cats during orthostatic AP changes.

Animals and surgical procedures. Animals were cared for in strict accordance with the "Guiding Principles for the Care and Use of Animals in the Field of Physiological Sciences," approved by the Physiological Society of Japan. Six adult cats of either sex, weighing

Address for reprint requests and other correspondence: M. Sugimachi, Dept. of Cardiovascular Dynamics, National Cardiovascular Center Research Institute, 5-7-1 Fujishirodai, Suita 565–8565, Japan.

The costs of publication of this article were defrayed in part by the payment of page charges. The article must therefore be hereby marked "*advertisement*" in accordance with 18 U.S.C. Section 1734 solely to indicate this fact.

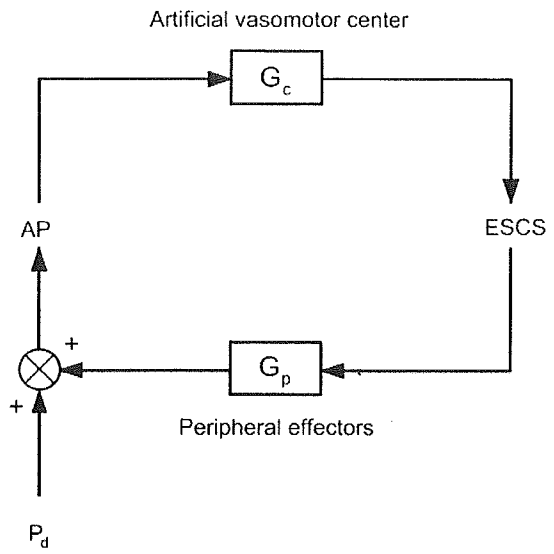

Fig. 1. Simplified diagram of bionic baroreflex system (BBS) using epidural spinal cord stimulation (ESCS). Peripheral effectors change arterial pressure (AP) in response to ESCS. The artificial vasomotor center determines ESCS rate in response to changes in AP. Transfer function of the peripheral effectors (G_p) cannot be controlled, but the vasomotor center transfer function (G_c) can be computer programmed as needed. P_d, pressure disturbance to AP.

1.6–3.7 kg, were premedicated with ketamine (5 mg/kg im) and then anesthetized by intraperitoneal injection (1.0 ml/kg) of a mixture of urethane (250 mg/ml) and α-chloralose (40 mg/ml).

For AP measurement, a high-fidelity pressure transducer (SPC-320, Millar Instruments, Houston, TX) was placed in the aortic arch via the right femoral artery. Pancronium bromide (0.3 mg/kg) was administered to prevent muscular activity. The cats were mechanically ventilated with oxygen-enriched room air. Body temperature was maintained at around 38°C with a heating pad. To produce the baroreflex failure model, the carotid sinus, aortic depressor, and vagal nerves were sectioned bilaterally. The rationale for using baroreceptor-deafferentiated animals as the baroreflex failure model is that, in patients with multiple-system atrophy, the reason for sudden hypotension induced by orthostatic change is a lack of reflex control of AP sensed at the baroreceptors.

A partial laminectomy was performed in the L_3 vertebra to expose the dura mater. A multielectrode catheter with interelectrode distance of 10 mm was introduced rostrally ~7 cm into the epidural space. The stimulating electrodes were positioned on the dorsal surface of the spinal cord within T_{12}, T_{13}, and L_1. These spinal levels were selected because our preliminary studies showed that ESCS to these levels produced greater AP response compared with other spinal levels. The catheter was connected to an isolated electric stimulator (SS-102J and SEN7203, Nihon Kohden, Tokyo, Japan) via a custom-made, constant-voltage amplifier. The stimulator was controlled with a laboratory computer (PC9801FA, NEC, Tokyo, Japan).

Data recording for characterizing AP response to ESCS. To characterize the static as well as dynamic AP responses to ESCS, we measured AP responses while changing ESCS rate. To estimate static response, we changed the ESCS rate sequentially in stepwise increments and decrements. Each stimulation step was maintained for 90 s. To estimate dynamic response, we randomly changed the ESCS rate, according to a binary white noise sequence with a minimum sequence length of 1 s. In both protocols, the stimulation voltage was fixed at 5 V, and the pulse width of the stimulus was 1 ms. While the stimulation was given, ESCS rate and AP were digitized at a rate of 200 Hz with a 12-bit resolution analog-to-digital converter [AD12–8 (PM), Contec, Osaka, Japan] and stored in another laboratory computer (PC98-NX VA70J, NEC). In this study, "ESCS rate" is defined as the number of stimulation pulses per second and is distinguished from the term "frequency," which refers to how frequently ESCS rate changes.

Estimation of static AP response parameters. We parameterized the static AP response to ESCS. Each steady-state AP value was obtained by averaging the AP during the last 10 s of each ESCS step. Stimulation at low-ESCS rate decreased AP, but stimulation at higher rates increased AP. We fit both responses together to a linear regression model of AP vs. ESCS rate. We determined the rate at which the pressor and depressor effects balanced and designated it the offset stimulation rate (s_o).

Estimation of peripheral effector transfer function. The transfer function of the peripheral effector was estimated by using a white noise method described in detail elsewhere (10, 13, 16, 24–26, 31). Briefly, on the basis of the resampled data at 10 Hz, the linear transfer function from ESCS rate to AP was calculated as a quotient of the ensemble average of cross-power between the two and that of ESCS rate power. The transfer function was calculated up to 0.5 Hz with a resolution of 0.0098 Hz. We parameterized the transfer function by using an iterative, nonlinear, least squares fitting technique (10).

Design of central characteristics and implementation by the artificial vasomotor center. Based on the parameterized effector transfer function, we designed the vasomotor center transfer function using computer simulation. The characteristics of the vasomotor center have been identified as derivative characteristics in rabbits and rats (10, 13, 25). We did not have the corresponding data for cats but assumed that they resembled those in rabbits and rats. We adjusted the parameters by simulation, aiming to attenuate hypotension to ~20 mmHg within 5 s and to ≤10 mmHg at 30 s. We implemented designed transfer function by the artificial vasomotor center with convolution algorithm (see APPENDIX).

Head-up tilt tests. The efficacy of the BBS against orthostatic stress was evaluated in each animal by the head-up tilt (HUT) test. We placed baroreflex failure animals in a prone position on a custom-made tilt table and measured AP responses to 60° HUT, with or without BBS activation. In the absence of BBS control, we fixed the ESCS rate at s_o, irrespective of AP changes. The BBS was activated by sending ESCS command to the stimulator, as calculated by the artificial vasomotor center in response to AP change. Tilt angle, ESCS rate, and AP were stored in a laboratory computer.

Statistical analysis. All data are presented as means ± SD. We analyzed AP responses at 5 and 30 s after HUT. AP changes from control value were compared among protocols by using repeated-measures analysis of variance followed by Dunnett's multiple-comparison procedure (8). Differences were considered significant when $P < 0.05$.

RESULTS

Figure 2*A* is a representative example of static AP response to stepwise ESCS changes. Stepwise increases of ESCS rate produced a depressor response initially at low-ESCS rate and a pressor response at higher rates, and subsequent decreases of ESCS rate produced almost perfect reversal of AP changes. The relationship between AP and ESCS rate appeared nonlinear as a whole (Fig. 2*B*, *top*). However, for ESCS rates of 2 pulses/s and above, there is a linear relationship ($r^2 = 0.964$, AP = 16.0 × ESCS + 44.0, s_o = 3.2 pulses/s; Fig. 2*B*). A linear relationship during ESCS was found in all animals [r^2, 0.876–0.979 (median, 0.959) slope, 14.3 ± 5.8 mmHg·pulses^{-1}·s; pressure axis intercept, 35.7 ± 25.6 mmHg; s_o, 4.9 ± 2.5 pulses/s]. The following protocols were performed by using this linear ESCS range.

Figure 3*A* is a representative example of dynamic AP response to ESCS. We selected low- and high-stimulation rates that produced depressor and pressor responses, respectively,

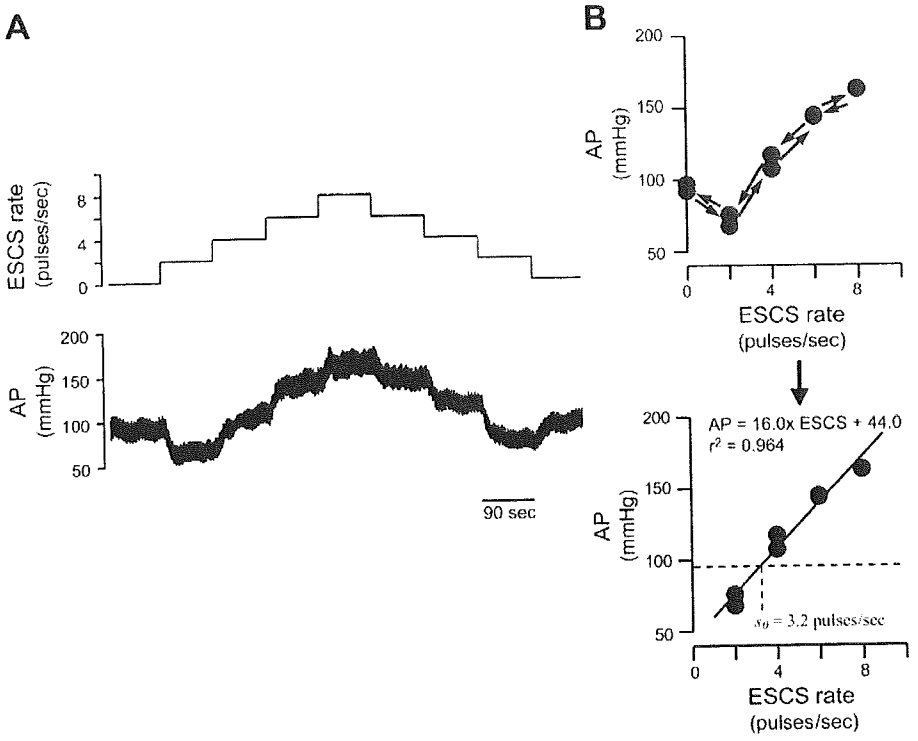

Fig. 2. *A*: representative time series of static AP response to ESCS. Stepwise increases of ESCS rate produced a depressor response initially at low-ESCS rate and a pressor response at higher rates, and subsequent decreases of ESCS rate produced almost perfect reversal of AP changes. *B*: procedures to estimate steady-state relationship between AP and ESCS rate. Each steady-state AP value was plotted against ESCS rate (*top*). Although the relationship between AP and ESCS rate appears nonlinear as a whole, linear regression analysis was conducted for the data obtained during ESCS (2, 4, 6, and 8 Hz), omitting the values before and after ESCS (0 Hz). A linear relationship is obtained. The value s_0 represents the stimulation rate where pressor and depressor responses balance.

and stimulated the spinal cord, according to a binary white noise sequence. AP did not respond to fast changes in ESCS rate, but appeared to respond to slower changes, increasing with high-rate stimulation and decreasing with low-rate stimulation. The estimated transfer function indicated low-pass filter characteristics. Figure 3*B* shows the averaged transfer function from ESCS rate to AP in six animals. The gain decreased as the frequency increased and was attenuated to one-tenth of the lowest frequency at 0.1 Hz. The phase approached zero radian at the lowest frequency, reflecting in-phase changes of ESCS rate and AP. The parameters obtained by the least squares fitting to the second-order, low-pass filter model are as follows: dynamic gain = 16.7 ± 8.3 mmHg·pulses^{-1}·s, natural frequency = 0.022 ± 0.007 Hz, damping coefficient = 2.40 ± 1.07, and lag time = 1.06 ± 0.41 s. The dynamic gain was much higher than the gain at the lowest frequency in the transfer function (Fig. 3*A*) but comparable to the slope obtained in the static protocol. The coherence function was close to unity between 0.01 and 0.4 Hz, indicating that the input-output relation was governed by almost linear

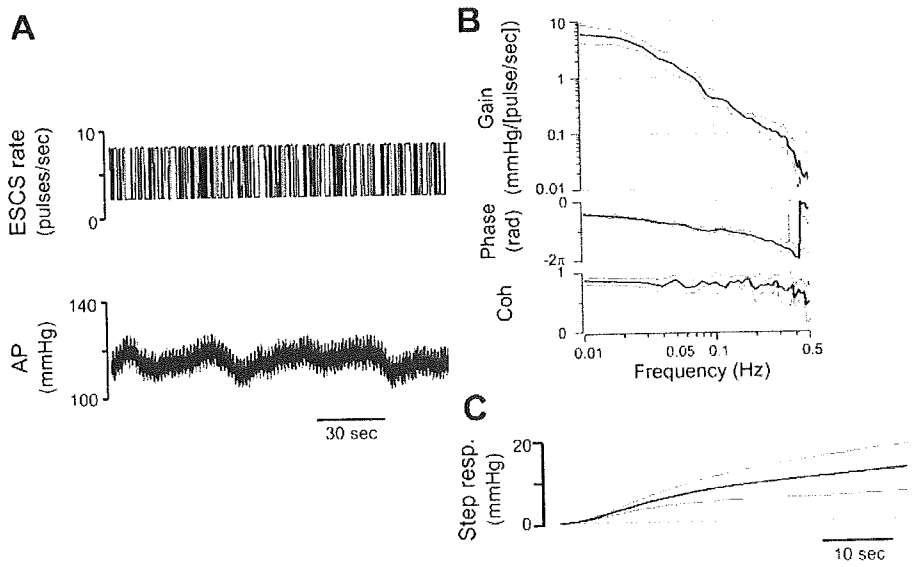

Fig. 3. *A*: representative example of dynamic AP response to ESCS. *B*: averaged transfer functions from ESCS rate to AP, i.e., G_p (gain and phase) and coherence function (Coh). *C*: estimated step response (resp) computed from the transfer function. Data are expressed as means ± SD for 6 cats.

dynamics in this range. To facilitate better understanding of the dynamic AP response to ESCS, the step functions were calculated by time integral of the inverse Fourier transform of the transfer functions. The estimated step functions are averaged and shown in Fig. 3*C*. An initial time lag and overdamped slow AP response to unit step ESCS are evident. The time courses of the estimated step functions were almost identical to but smoother than those of the actually observed AP responses to stepwise ESCS changes, indicating the ability to cancel out noises by the white noise method.

Figure 4 is a representative example of how we designed the vasomotor center transfer function. The steady-state gain is determined simply to match a total baroreflex loop gain of 5. This setting ensures that the steady-state AP fall will be attenuated to 10 mmHg in the case of a depressor stimulus of 60 mmHg. By changing the derivative corner frequency (f_c), we simulated various transient AP responses to orthostatic depressor stimulation. Lower f_c causes unstable oscillation in AP (Fig. 4*B*, *left*), and higher f_c slows AP restoration (Fig. 4*B*, *right*). On the basis of these simulations, f_c = 0.02 Hz was selected in this example (Fig. 4*B*, *middle*, 0.018 ± 0.008 Hz in 6 cats).

Figure 5 shows a representative example of real-time application of BBS to a cat. In the control cat with baroreflex failure, abrupt HUT produced a rapid and then progressive fall in AP by 44 mmHg in 30 s (Fig. 5, *left*). Activation of the simulation-based BBS attenuated the AP fall (Fig. 5, *middle*; AP fall, 25 mmHg in 5 s and 19 mmHg in 30 s) but did not attain the predetermined target (gaps indicated by vertical bars in Fig. 5, *middle* and *right*). If the total loop gain of 5 were preserved, the AP fall should theoretically be attenuated to 44/(1 + 5), or ~7 mmHg, according to the linear control theory. The observed attenuation of 19/44 (=1/2.3) indicated that the actual gain was 1.3 (1 + 1.3 = 2.3). To achieve a total loop gain of 5, we increased the gain of the vasomotor center transfer function by 3.8-fold and reassessed the efficacy of BBS. As a result, AP returned to the predetermined target (Fig. 5, *right*; AP fall, 19 mmHg in 5 s, 7 mmHg in 30 s).

Figure 6 summarizes the results obtained from six cats, demonstrating the effectiveness of the BBS performance. In the cat model of baroreflex failure, HUT decreased AP by 37 ± 5 mmHg in 5 s and by 59 ± 11 mmHg in 30 s. In animals with simulation-based vasomotor center, the initial attenuation (AP fall: 32 ± 7 mmHg in 5 s) was not significant, and the steady-state attenuation (17 ± 8 mmHg in 30 s) did not satisfy the predetermined target. On the other hand, in animals with gain-adjusted vasomotor center (2.4 ± 1.1-fold increase), the BBS achieved both initial and the steady-state targets (21 ± 2 mmHg in 5 s, $P < 0.05$; 8 ± 4 mmHg in 30 s, $P < 0.05$).

DISCUSSION

The present results indicate that AP can be controlled by ESCS and that ESCS-mediated BBS prevents orthostatic hypotension in anesthetized cats. Although the BBS based on simulation alone did not work as predicted during HUT, gain adjustments of the vasomotor center achieved quick and stable restoration of AP.

Necessity of BBS for treatment of central baroreflex failure. Conventional treatments for central baroreflex failure aim at increasing AP. Although they alleviate the hypotension to the extent of preventing syncope, they have adverse effects of causing supine hypertension and enhancing the risk of hypertensive organ disease. Recently, Shannon et al. (28) suggested well-timed water consumption as a treatment for orthostatic hypotension in patients with autonomic failure. Their strategy is superior to conventional treatments because it prevents AP fall if predicted in advance. However, at least a few minutes are necessary for their method to increase AP. This time lag makes it impossible to control AP against sudden or unpredictable AP

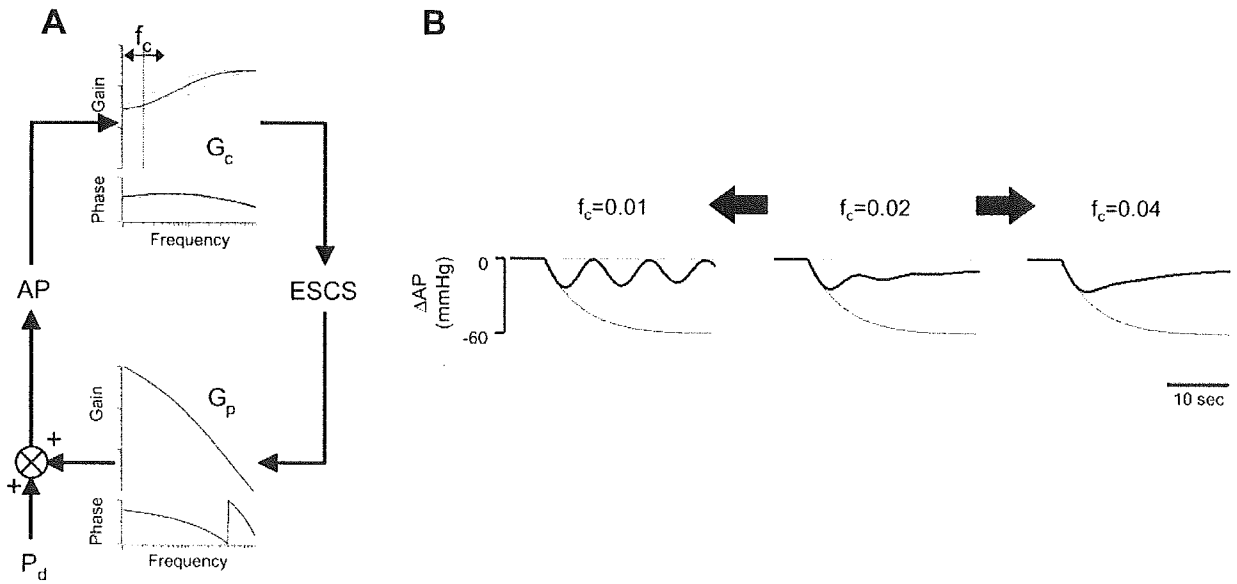

Fig. 4. Representative example of designing the G_c. *A*: schematic diagram of the method of designing the G_c. AP changes in the presence of P_d were simulated by changing the corner frequency (f_c) for derivative characteristic in the G_c. *B*: simulation results of this example. A vasomotor center with f_c of 0.02 Hz restores AP with sufficient speed and stability (center).

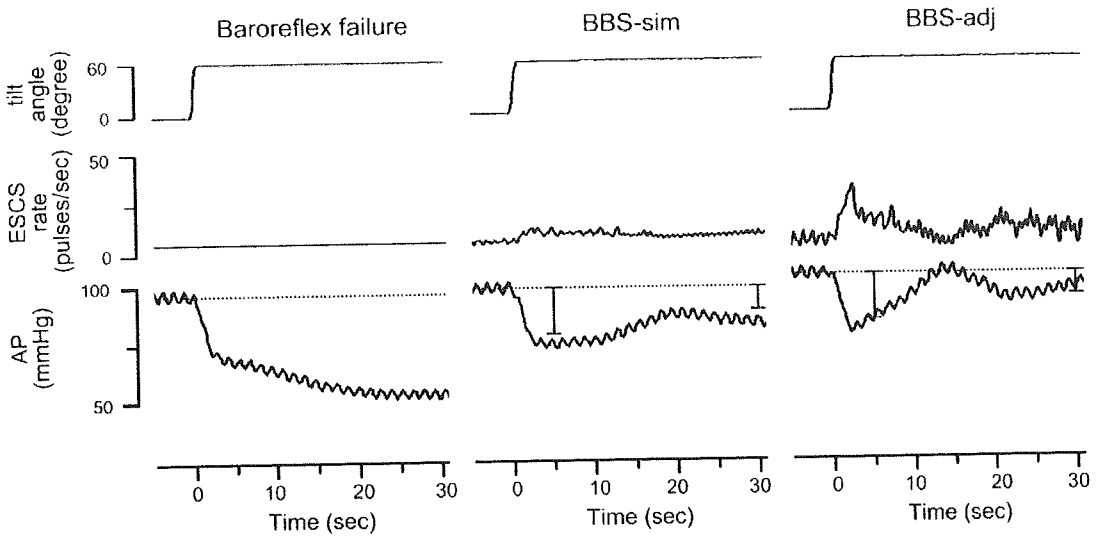

Fig. 5. Representative example of real-time application of the BBS during head-up tilt (HUT). *Left*: in the cat with baroreflex failure, ESCS rate was fixed at 5.0 pulse/s. HUT produced a rapid and then progressive fall in AP. *Middle*: simulation-based BBS (BBS-sim) attenuated the AP fall but did not attain the predetermined target. *Right*: gain adjustment of the vasomotor center (BBS-adj) resulted in quick and sufficient attenuation of AP fall (see text for detail). Vertical bars indicate the ranges of predetermined targets.

fall. None of the treatments attempted so far can prevent sudden orthostatic hypotension because the dynamics of the baroreflex remain impaired.

In contrast, the BBS continuously monitors and controls AP to achieve quick restoration of AP. Because AP is increased via sympathetic pathways, the AP response to the BBS vasomotor center command is as fast as that to the native vasomotor center control. Therefore, the quick, adequate, and stable nature of the native baroreflex system can be restored by the BBS with appropriate settings of the artificial vasomotor center.

Designing the vasomotor center transfer function and parameter adjustments. In a negative feedback system, closed-loop responses to external perturbation are dependent on the dynamic characteristics of the total open-loop transfer function. We assumed that the derivative characteristics in cats are identical to those in rabbits or rats, which have been delineated previously (10, 13, 25). We optimized gain and derivative parameters for each cat so that both speed and stability were achieved.

In animal experiments, however, the simulation results were not fully reproduced. Gain adjustments of the vasomotor center were necessary to attain quick and sufficient attenuation of the AP fall. This discrepancy cannot be explained without considering a possible slope decrease or nonlinearity in peripheral effector characteristics (AP-ESCS relationship) caused by the HUT, or both. Pooling of blood volume in the splanchnic and hindlimb circulation would be a cause for such attenuated AP response. If AP responses during posture change can be de-

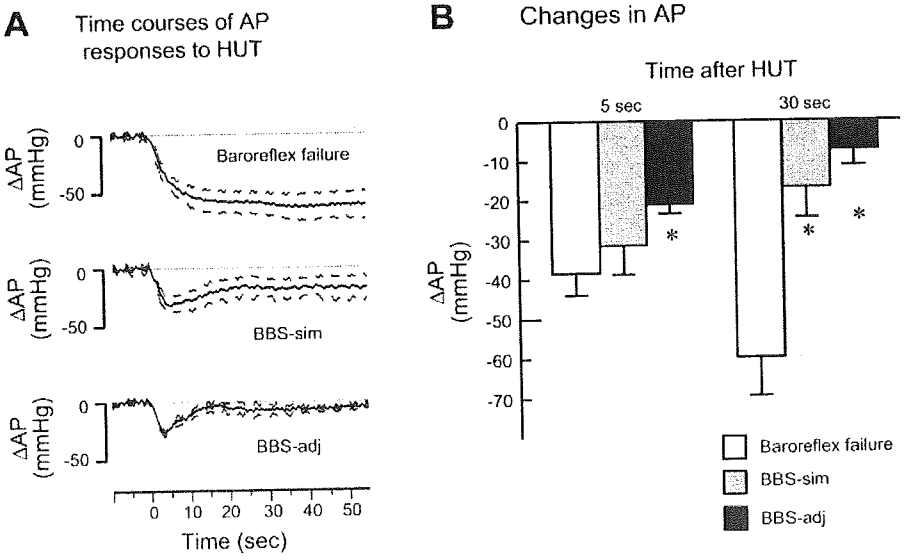

Fig. 6. Summarized results of HUT obtained from 6 cats. *A*: averaged time courses of AP responses to HUT in cats with baroreflex failure (*top*) and with BBS (*middle* and *bottom*). Using the parameters determined from simulation, we found that the BBS (BBS-sim) did not adequately attenuate hypotension in all cats (*middle*). Appropriate gain increase (BBS-adj) was necessary for quick and sufficient attenuation of hypotension (*bottom*). *B*: changes in AP produced by HUT. Data are expressed as means ± SD. $^*P < 0.05$ compared with baroreflex failure.